Calcar femorale variation in extant and fossil hominids: Implications for identifying bipedal locomotion in fossil hominins

Marine Cazenave [a,b,*], Tracy L. Kivell [a,c,d], Marta Pina [e,f], David R. Begun [g], Matthew M. Skinner [a,c,d]

[a] *Skeletal Biology Research Centre, School of Anthropology and Conservation, University of Kent, Canterbury, UK*

[b] *Department of Anatomy, Faculty of Health Sciences, University of Pretoria, South Africa*

[c] *Department of Human Evolution, Max Planck Institute for Evolutionary Anthropology, Leipzig, Germany*

[d] *Centre for the Exploration of the Deep Human Journey, University of the Witwatersrand, Johannesburg, South Africa*

[e] *Interdisciplinary Centre for Ancient Life, School of Natural Sciences, University of Manchester, Manchester, UK*

[f] *Institut Català de Paleontologia Miquel Crusafont, Universitat Autònoma de Barcelona, Cerdanyola del Vallès, Spain*

[g] *Department of Anthropology, University of Toronto, Toronto, Ontario, Canada*

Corresponding author.

Email address: marine.cazenave4@gmail.com (M. Cazenave)

Calcar femorale variation in extant and fossil hominids: Implications for identifying bipedal locomotion in fossil hominins

Abstract

The calcar femorale is an internal bony structure of the proximal femur considered to be functionally related to bipedal locomotion. Among extant primates, the presence of a calcar femorale has been so far documented in extant humans and *Pan* and, among extinct hominins, in the late Miocene *Orrorin*, in a Pliocene *Australopithecus*, and in a Middle Pleistocene *Homo* specimen. Using high-resolution microcomputed tomography, we investigated the occurrence and morphology (i.e., shape, location, and size) of the calcar femorale in an adult sample of extant humans, *Pan troglodytes*, *Gorilla gorilla*, *Pongo* sp., and *Papio ursinus*. We also investigated for the first time the occurrence and morphology of a calcar femorale in the adult proximal femoral remains of a late Miocene great ape (*Rudapithecus*) and five Plio-Pleistocene hominins from Southern and Eastern Africa (*Australopithecus* and *Paranthropus*). We took four measurements: periosteal-to-tip maximum length, maximum length excluding cortical thickness, maximum vertical height, and the distance between the most anterior and posterior limits of the root. To allow for intergeneric comparisons, estimated body size was used to standardize all measurements. Nine of 10 extant humans have a well-developed calcar femorale. Among the African apes, 6/10 *Pan* and 6/10 *Gorilla* also show a distinct calcar femorale. In *Pongo* (n = 9), it is only present in one captive individual. None of the five investigated *Papio* specimens show any trace of this structure. Only calcar femorale height, which is systematically taller and extends into the lower part of the lesser trochanter, discriminates humans from extant great apes, except for one *Gorilla*. The calcar femorale was absent in one *Paranthropus robustus* and variably developed in all other investigated

fossils. These results indicate that this structure cannot be considered as a diagnostic feature of habitual bipedal locomotion and emphasize the need for further investigations of its functional role.

Keywords: Proximal femur; Extant great apes;; X-ray microtomography; Internal bone structure; calcar femorale occurrence, calcar femorale morphology

1. Introduction

The calcar femorale (CF) is an osteological feature described in a typical, healthy human femur as a vertical to slightly oblique spur of thickened bone within the femoral neck (Fig. 1). It typically extends from the inferolateral endosteal margin of the femoral neck, posterior to the neutral axis, laterally and distally towards the greater trochanter (Griffin, 1982; Adam et al., 2001; Le Corroller et al., 2011). The CF was illustrated for the first time in a mid-19th century human anatomical atlas (Pirogovs, 1853, as cited by Glinkowski and Ciszek, 1989). Since then, the gross morphology and possible functional significance of the CF, especially in relation to bipedalism, have been discussed in several anatomical studies (e.g., Merkel, 1874; Bigelow, 1875; Dixon, 1910; Harty, 1957; Griffin, 1982; Stiles et al., 1990; Hammer, 2019) and increasingly considered in clinical research, particularly in relation to osteoporosis and osteoarthritis (e.g., Le Corroller et al., 2011; Thakkar et al., 2015; Tetsunaga et al., 2017; Sas et al., 2019; Zha et al., 2019).

The CF is thought to be related to the load created by the insertion of the iliopsoas tendon on the lesser trochanter (Cunningham et al., 2016) and experimental and clinical studies have identified that it provides additional mechanical strength for weight transmission (Li and Aspden, 1998; Zhang et al., 2009). The CF is proximally rooted at the region of bending of the neck-shaft arch and therefore is thought to act as a transitional structure for load transfer through the hip joint and to prevent the posterior and medial regions of the proximal femur from suffering overload (Farkas et al., 1948; Li and Aspden, 1997, 1998; Gao et al., 1999; Wang et al. 2005; Zhang et al., 2009; Hammer, 2019). In addition, it is architecturally connected with the vertical and the trochanteric trabecular bundles (Aiello and Dean, 1990). The vertical bundle arises from the superior aspect of the head and radiates inferolaterally towards the inferior cortex of the femoral neck, while the trochanteric bundle radiates towards the medial cortex of the shaft by forming a

‘Gothic arch’ at the intersection with the arcuate bundle (see Cazenave et al., 2021: Figure 6; Kapandji, 2011). As review in Kapandji (2011) and Levangie and Norkin (2011), these bundles reflect compressive and tensile stress trajectories through the human femoral neck created by axial compressive and bending loads. It is thought that the presence of a CF connected to the two bundles contributes to the strength of the base of the femoral neck in resisting these loads (Newell, 1997; Wroblewski et al., 2000; Hammer, 2010, 2019; Cunningham et al., 2016). However, morphostructural variability in the CF in extant humans has been reported across multiple age cohorts (Farkas et al., 1948). In addition to the occasional absence of this spur of thickened bone in both adult males and females, the CF can vary in adult individuals in shape and dimension, most notably in how far it penetrates within the lesser trochanter and the degree of intra-individual bilateral asymmetry (e.g., Thompson, 1907; Garden, 1961; Kuperavage, 2009; Hammer, 2010, 2019; Le Corroller et al., 2011; Kuperavage et al., 2018).

Experimental analyses have demonstrated that, within the limits imposed by a phylogenetically-determined adaptive Bauplan and the influence of a number of biological factors (e.g., hormones, cytokines, protein that regulate bone cells activity; Lovejoy et al., 1999; Judex et al., 2004; Demissie et al., 2007; Havill et al., 2007, 2010; Bonewald and Johnson, 2008; O’Neill and Dobson, 2008; Cunningham and Black, 2009; Estrada et al., 2012; Reissis and Abel, 2012; Wallace et al., 2012, 2020; Medina-Gomez et al., 2018; Hou et al., 2020), cortical bone thickness distribution and trabecular structure can adapt to the site-specific mechanical loading environment to resist local stresses (e.g., Lanyon, 1973; Skerry and Lanyon, 1995; Biewener et al., 1996; Guldberg et al., 1997; Mori et al., 2003; Mittra et al., 2005; Pontzer et al., 2006; Carlson and Judex, 2007; Chang et al., 2008; Polk et al., 2008; Barak et al., 2011; Wallace et al., 2013; Cresswell et al., 2015; Vera et al., 2020). Importantly, several studies have found that variation in cortical and/or trabecular

bone structure at different skeletal sites is consistent with predicted differences in locomotor-related loadings in humans and other primates. Indeed, although the link between the endostructural architecture of the proximal femur and the load transfer and dissipation is more complex than assumed by the first mechanical models (e.g., Fajardo et al., 2007; Ryan and Walker, 2010; Shaw and Ryan, 2012), trabecular bone variation in the primate femoral head has provided evidence for structural differences across locomotor groups and has identified unique features in humans related to habitual bipedalism (Fajardo and Müller, 2001; MacLatchy and Müller, 2002; Ryan and Ketcham, 2002a, b, 2005; Ryan and Krovitz, 2006; Saparin et al., 2011; Ryan and Shaw, 2012, 2015; Raichlen et al., 2015; Ryan et al., 2018; Tsegai et al., 2018a; Georgiou et al., 2019). Similarly, the asymmetrical distribution of cortical bone thickness within the femoral neck compartment, resulting from an absolutely thinner superior cortex and a thicker inferior cortex, has been shown to similarly characterize bipedal humans and quadrupedal primates, reflecting their stereotypical loadings at the hip joint (Lovejoy, 1988, 2005; Ohman, 1993; Ohman et al., 1997; Rafferty, 1998; Lovejoy et al., 2002; Ruff and Higgins, 2013; Ruff et al., 2016; Cazenave et al., 2019; Pina et al., 2019). However, compared to the femoral head and neck, other anatomical regions of the proximal femur have received far less attention in extant humans and other primates (Miller et al., 2002; Cazenave et al., 2021).

In nonprimate animals, the CF was found to be absent in small samples of hens, dogs, and pigs (Glinkowski and Ciszek, 1989). Among primates, the presence of a CF has thus far only been investigated in a sample of 10 rhesus macaques, where it was reportedly absent in all individuals (Glinkowski and Ciszek, 1989), and in chimpanzees (*Pan troglodytes*), where it was identified in 7/10 individuals (Kuperavage et al., 2018). However, in chimpanzees, the CF was found to be distinguishable from the human condition due to both a lower occurrence and because of a more

limited vertical extension within the femoral neck (Kuperavage et al., 2018). Recently, it has been reported that some *Gorilla* specimens also exhibit a calcar femorale (e.g., KUPRI 1492 on the Kyoto University Digital Morphology Museum site; pers. commun. to R. H. Crompton from A. Kuperavage; Crompton et al., 2021), but neither quantitative evidence nor images have been provided.

Because of the presumed mechanical relationship of the CF to bipedalism, its occurrence (i.e., presence or absence) has also been investigated in some early fossil hominins (White, 1984; Grine et al., 1995; Kuperavage et al., 2018). The presence of a CF was reported in the late Miocene *Orrorin tugenensis* (BAR 1002'00 and 1003'00; Kuperavage et al., 2018) and, because of its relative vertical extension, has been invoked to support the inference of bipedal locomotion in this taxon (Senut et al., 2001; Pickford et al., 2002). A CF has also been identified in an *Australopithecus* specimen (MAK-VP-1/1; White, 1984; see also Reed et al., 1993) and in a Middle Pleistocene *Homo* specimen (Berg Aukas; Grine et al., 1995). However, to date, no study has evaluated the occurrence of the CF in any extinct nonhuman hominid. Given the variability in occurrence and morphology of the CF observed in extant humans, the very limited data for extant nonhuman primates, and the lack of information on this feature in extinct hominids, a more detailed consideration of the CF in extant and fossil primates may provide greater clarity on its functional significance and whether there are unique aspects of this feature that could potentially be related to bipedalism.

To address these knowledge gaps, we use high-resolution microcomputed tomography (μCT) to evaluate and compare CF occurrence and three-dimensional (3D) morphology (i.e., shape, location, extension within the lesser trochanter, absolute and standardized horizontal length and vertical height, and root width) in adult femora representing extant humans, extant great apes (*Pan*,

Gorilla, and *Pongo*), and one species of cercopithecine monkey (*Papio*). We then evaluate CF occurrence and morphology in the adult femoral remains of a late Miocene great ape (*Rudapithecus*) and five Plio-Pleistocene hominins from Southern and Eastern Africa representing *Australopithecus* and *Paranthropus*. We expand on previous studies by not only assessing CF occurrence and morphology in a broader taxonomic extant and extinct primate sample, but also by quantifying additional aspects of the CF, i.e., CF length excluding the cortex to assess the influence of variation in cortical bone thickness, and CF maximum vertical height and root thickness to determine whether the degree of development of such parameters is unique to habitual bipeds. Based on the body of evidence available thus far, we hypothesize that 1) extant humans and great apes differ in CF occurrence and morphology, and both differ from the pattern observed in *Papio*; 2) extinct hominins are more similar in CF occurrence and morphology to that of extant humans compared with other extant apes, and 3) the Miocene ape *Rudapithecus* is most similar to the CF morphology to extant apes. Below we outline our predictions.

Assuming the CF is primarily, though not necessarily uniquely related to mechanical loading during bipedal behaviors (Farkas et al., 1948; White, 1984; Reed et al., 1993; Grine et al., 1995: Kuperavage et al., 2018; Hammer, 2019), and given the results of human and *Pan* comparisons presented in Kuperavage et al. (2018), we predict that the CF will be more frequently expressed, absolutely and relatively longer, more vertically extended, and characterized by a thicker root, in our sample of extant humans compared to the extant ape and *Papio* samples.

Although extant great apes differ in their type and frequency of locomotor and postural behaviors (primarily knuckle walking in the African apes vs. specialized suspensory behaviors in orangutans; e.g., Hunt, 1991; Doran, 1996; Thorpe and Crompton, 2006; see also Almécija et al., 2021 for a review), they share a high degree of hip joint mobility with enhanced abduction and

lateral rotation movements (Isler and Thorpe, 2003; Hammond, 2013; Finestone et al., 2018). Moreover, great apes show similar patterns of trabecular bone distribution within the femoral head (Ryan and Shaw, 2012; Georgiou et al., 2019) and similar arrangement of cortical and trabecular bone at the neck/shaft junction, suggesting that *Pan*, *Gorilla*, and *Pongo* experience generally comparable load transfer at the hip joint (Rafferty, 1998; Cazenave et al., 2019; Pina et al., 2019). We therefore predict a similar degree of development of the CF (i.e., occurrence, shape, extension into the lesser trochanter, absolute and relative vertical length, height and root width) within the three great apes. In contrast, *Papio*, which engages primarily in terrestrial, pronograde quadrupedal walking and running (Rose, 1977), has a lower hip joint mobility than that of great apes (Hammond, 2013), which is reflected in a more asymmetrical distribution of cortical bone in the femoral neck (Rafferty, 1998; Pina et al., 2019). Thus, we predict that the CF should not be present in *Papio.*

Australopithecines are considered habitual bipeds when terrestrial (Ward, 2013), although likely somewhat distinct from humans in their bipedal biomechanics and loading environment at the hip joint (e.g., Ruff and Higgins, 2013; Ryan et al., 2018; Cazenave et al., 2019, 2021). It is thus expected that australopithecines express a CF configuration (i.e., shape, location, extension within the lesser trochanter, absolute and standardized horizontal length and vertical height, and root width) similar to the extant human condition. In contrast, *Rudapithecus*, the only fossil ape analyzed in this study, has postcranial morphology suggesting frequent use of forelimb-dominated suspensory behaviors (Morbeck, 1983; Begun, 1993; Kivell and Begun, 2009; Ward et al., 2019; Almécija et al., 2021). Thus, if a CF is present in *Rudapithecus*, we expect its morphology to be most similar to that of extant great apes.

2. Materials and methods

2.1. Samples

Our extant primate sample consists of 44 femora from adult males and females of modern humans (*n* = 10), *Pan troglodytes* (*n* = 10), *Gorilla gorilla* (*n* = 10), *Pongo* sp. (*n* = 9), and *Papio ursinus* (*n* = 5). All specimens were free from obvious signs of pathology. All nonhuman primate specimens were wild caught, with the exception of two captive *Pongo* specimens. Six *P. troglodytes* and one *Pongo* specimens were of unknown provenance. Details of the extant sample composition are provided in Supplementary Online Material (SOM) Table S1.

We included one fossil great ape specimen representing *Rudapithecus hungaricus* (RUD 234) from the late Miocene site of Rudabánya (Hungary), housed at the Mining and Geological Survey of Hungary, Budapest (Begun et al., 2012; Ward et al., 2019; SOM Table S2). The Plio-Pleistocene hominin sample includes the following specimens: StW 99 and 367 from Sterkfontein Member 4, South Africa, both attributed to *Australopithecus africanus* and curated at the Evolutionary Studies Institute of the University of the Witwatersrand, Johannesburg, South Africa (Harmon, 2009; Ruff and Higgins, 2013; Zipfel et al., 2020; Pickering et al., 2021); SK 97 from Swartkrans Member 1, South Africa representing *Paranthropus robustus* curated at the Ditsong National Museum of Natural History, Pretoria, South Africa (Robinson, 1972; Susman et al., 2001; Cazenave et al., 2019, 2021); and KNM-ER 738 and 1465 from Koobi Fora, Kenya, both likely representing *Paranthropus boisei* curated at the National Museums of Kenya, Nairobi (Wood and Costantino, 2007; Wood and Leakey, 2011; Ward et al., 2015; Ruff et al., 2016; SOM Table S2). We also assessed additional fossil specimens including four Miocene apes (including one *Dryopithecus fontani*, two *Hispanopithecus laietanus*, and another *R. hungaricus* femora) and five Plio-

Pleistocene hominins (representing three additional *A. africanus*, one *P. robustus* and one *P. boisei* or *Homo* sp.); however, their poor internal preservation prevented the possibility to reliably quantify potential CF morphology (SOM Table S2; SOM Fig. S1).

2.2. Microcomputed tomography

Details on the different microtomographic (µCT) equipment and the scanning resolutions are provided in SOM Tables S1 and S2 for the extant and the fossil specimens, respectively. Four individuals of the extant human sample and one *Pan* femur were scanned using a Nikon XT H225/320L industrial XCT system at the Evolutionary Studies Institute of the University of the Witwatersrand (Johannesburg, South Africa) using 70 kV, 120 µA, and 2000 projections. The remaining human specimens and one *Papio* specimen were scanned at the microfocus X-ray tomography facility (MIXRAD) of the South African Nuclear Energy Corporation SOC Ltd (Necsa, Pelindaba), using a Nikon XTH 225 ST (Metris) equipment and 100 kV, 100 µA, and 1000–2000 projections. Seven *Pan* specimens were scanned at the AST-RX: X-ray tomography technical platform by the v|tome|x L 240–180 equipment housed at the Muséum National d'Histoire Naturelle (Paris, France) using 100 kV, a current ranging from 500 to 610 µA, and 2400–2900 projections. The two remaining *Pan* specimens, the *Pongo* sample, and all fossil specimens were scanned with the BIR ACTIS 225/300 industrial microfocus X-ray tomography scanner at the Department of Human Evolution in the Max Planck Institute for Evolutionary Anthropology (Leipzig, Germany), using 130–140 kV, 100–140 µA, and 2500–2790 projections. The *Gorilla* sample was scanned with a Nikon XT 225 ST Metris scanner at the Cambridge Biotomography Centre of the Department of Zoology, University of Cambridge (Cambridge, UK) at 145–170 kV, 110–160 µA, and 2000 projections. Details about the scanning procedures used to image the

additional nine fossil specimens that were excluded from the study due to poor preservation are provided in SOM Table S2.

Femur size varied greatly across our comparative sample, ranging from the smallest *Papio* to the largest *Gorilla*. Thus, scan resolution varied as well due to the constraints of the μCT systems and taking into account the specific geometric characteristics of the analytical platforms. The resolution range for each taxonomic sample was as follows: humans, 50–70 μm; *Pan*, 30–80 μm; *Gorilla*, 45–75 μm; *Pongo*, 28–29 μm; *Papio*, 45–67 μm. The fossil specimens were scanned at resolutions ranging from 30 to 91 μm (SOM Table S2).

Previous quantitative analyses of the CF in humans and *Pan* indicate that, when present, this spur of thickened bone measures several centimeters vertically and transversely (e.g., Kuperavage, 2009; Le Corroller et al., 2011; Tetsunaga et al., 2017; Kuperavage et al., 2018). Accordingly, potential measurement bias of the CF due to differences in μCT resolution or technical differences across scanning facilities is negligible (for comparative measurements of the μ-scale sized trabecular struts see Cazenave et al., 2021). For instance, if we consider a CF length of 7.76 mm in a *Pan* individual scanned with a resolution of 80 μ (i.e., the lowest resolution used in the present study), a measurement error of 1 pixel would represent only 1.03% of the length of the CF (i.e., 0.08 mm).

All specimens were virtually rotated to the same anatomical position in Avizo v. 9.0.0 (Visualization Sciences Group Inc., Bordeaux) by using the neck axis and the principal axis of the proximal shaft portion as anatomical references. Left-side specimens were flipped so all specimens were analyzed as right femora.

2.3. Measurements and analyses

To assess the occurrence and, when present, the variation in morphology of the CF across our sample, we placed a transverse cross section at the level of the upper margin of the lesser trochanter and then virtually moved proximally towards the dorsomedial neck region and distally across the lesser trochanter. When the presence of the CF was identified, we placed a parasagittal cross section at the level of the center of the lesser trochanter and virtually moved mediolaterally to delimit the extent of the CF. In the specimens showing at least a trace of the bony spur, we characterized the shape of the CF according to the three categories established by Le Corroler et al. (2011): 1) a relatively short and thick ridge-like CF, 2) a spur-type CF, or 3) a relatively thin and long septum-like CF.

To test our predictions of a longer and more vertically extended CF with a wider root in extant and fossil hominins compared with the extant and fossil great apes, and of a similar degree of development (i.e., vertical extension, absolute and relative vertical length and height, and root width thickness) among the great ape taxa, we automatically segmented the cortex from the trabecular bone using the software Dragonfly v. 2020.2.0.941 (Object Research Systems Inc., Montreal) and the method developed by Buie et al. (2007). The CF was virtually extracted from the cortex for 3D rendering. Due to preservation, the CF from fossil specimens could not be automatically segmented and was completed manually instead. We first qualitatively compared the extent of the CF into the lesser trochanter and we took the following CF measurements: maximum length, maximum vertical height and maximum root width.

We used two methods to assess CF maximum length. In all extant specimens, the distance between the periosteal surface and the most internal point (the tip) of the CF (PT MaxLength) was automatically computed using the ‘Surface Distance’ module in Avizo v. 9.0.0 and then rendered in 3D using a chromatic scale where the outer contour-tip distance increases from dark blue (thin)

to red (thick; Fig. 2a). However, for the six fossil specimens, we could not automatically quantify the distance from the periosteal surface due to poor preservation. In these specimens, we manually measured CF maximum length (CF MaxLength) from the base lying on the endosteal contour (the root) to the tip of its most lateral extension, thus excluding the cortical thickness (Fig. 2b). Given that multiple factors have been shown in humans to affect cortical thickness variation throughout life (e.g., Gocha and Agnew, 2016), we also quantified CF MaxLength (length excluding the cortical bone) in all extant specimens for direct comparison with the fossil specimens. We found a high Spearman's rank correlation coefficient between PT MaxLength and CF MaxLength across the extant sample ($r = 0.91$, $p < 0.0001$). Calcar femorale maximum vertical height (CF MaxHeight) was measured as the vertical distance between the uppermost and lowest extracted slices bearing evidence of a CF-related spur of thickened bone, i.e., between the parallel planes orthogonal to the principal axis of the proximal shaft where the CF merges with the cortical bone of the posterior wall of the neck and the endosteal surface of the posterior wall of the diaphysis (Fig. 2c). Finally, in all cases where the most anterior and posterior limits of the CF root on the endosteal contour were clearly identifiable ($n = 18$ specimens), we also measured maximum CF root width on the related transverse cross section (Fig. 2d).

To allow for comparisons among extant taxa that differ in body size, all measurements were standardized by body mass. Body mass was estimated for each extant individual using the superoinferior diameter of the femoral head and the equations provided in Ruff et al. (2018) for the extant human sample and in Burgess et al. (2018) for the extant great ape taxa. Interspecific comparisons were completed on both the absolute and standardized mean values of each taxon. However, due to poor preservation of the femoral head, measurements of the fossils could not be standardized. Thus, all fossil results are presented and compared as absolute values only.

Given that cortical bone thickness at the base of the neck in extant apes and Neotropical monkeys has been shown to be influenced by loading conditions at this anatomical site (Ohman, 1993; Ohman et al., 1997; Rafferty, 1998), we additionally tested whether CF size correlates with variation in cortical thickness at this specific site. We measured cortical bone thickness (CBT) at the level of the most anterior (CBTa) and most posterior (CBTp) limits of the CF root in our extant sample (SOM Fig. S2) and used the average between the two as our estimate of CBT. We tested the possible influence of CBT variation on the CF parameters (i.e., CF length, vertical height, and root width) using a partial Spearman's correlation test controlling for body mass between CBT and each CF measurement. We also tested for the human, *Pan*, and *Gorilla* samples the possible influence within each species of body mass on CF length and vertical height using Spearman's correlation test. Given the sample size (n = 18), we could not test the possible influence of body mass on CF root width for the entire sample or all CF parameters in *Pongo* (n = 1).

All measurements used in this study were taken by one observer (M.C.). To examine the accuracy of the non-automated variables (i.e., CF MaxLength and CF MaxHeight), M.C. measured twice these variables in 50% of the specimens, another observer also measured these same variables in 50% of the specimens and intra- and interobserver tests were run, calculating the intraclass correlation coefficient (ICC) between the two sets of measurements. The results show an intraobserver ICC of 0.98 and 0.99 and an interobserver ICC of 0.78 and 0.85 for CF MaxLength and CF MaxHeight, respectively, indicating high reproducibility of the measurements. No interobserver tests were performed for CF root width, but repeated intraobserver measurements provided a highly satisfactory ICC of 0.93.

All statistical analyses and plots were performed in RStudio v. 1.2.5033 running with R v. 3.4.4 (R Core Team, 2018). Plots were generated using ggplot2 (Wickham, 2009). Due to small sample

sizes, only nonparametric tests were performed. Tests of significant interspecific differences in PT MaxLength, CF MaxLength, and CF MaxHeight (both absolute and standardized values) were conducted using the pairwise Wilcoxon rank sum test (alpha = 0.05). Given the small sample size, interspecific differences in maximum CF root width could not been carried out and males and females were combined for the analyses.

3. Results

3.1. Calcar femorale in the extant primate sample

Nine of the 10 extant humans (3 males and 6 females) showed the presence of a thick, ridge-like CF; a CF was absent in a 30–49 year-old male (Fig. 3a). Among the great apes, 6/10 *Pan* (4 males and 2 females) and 6/10 *Gorilla* (4 males and 2 females) expressed a bony spur ranging from a only ridge-like trace of this spur to a distinct septum-like structure. In *Pongo*, a CF was unambiguously found in one of the two captive males (Fig. 3e; SOM Table S1) and a CF ridge-like structure was also present in one wild *Pongo* female (Fig. 3d). In contrast, none of the *Papio* specimens showed a CF or a CF-like structure (Fig. 3; SOM Fig. S3).

In all specimens and taxa where the CF was present, it was located within the region spanning from the posteroinferior surface of the femoral neck to the lesser trochanter (Fig. 4). However, we observed intra- and interspecific variation in CF shape, extent, and size (both mediolaterally and proximodistally). In nearly all cases, the CF progressively thinned medially towards the tip, where it merged into the surrounding trabecular network with a tree-like pattern (SOM Fig. S3). However, CF thickness and density were variable, with some individuals, most notably in humans, displaying a plate-like structure resulting from the merging of thickened trabeculae rather than a

true spur of dense bone. In no case in our human sample did the CF extend to the posterior wall of the greater trochanter (Fig. 3; SOM Fig. S3). In some *Pan* and *Gorilla* (SOM Fig. S4), as well as in the *Pongo* individual displaying the CF (Fig. 3e), a variably-developed bone reinforcement emerging from the lateral margin of the lesser trochanter and radiating medially towards the CF was observed in the transverse slices. We did not observe a similar feature in our sample of human femora.

In extant humans, the CF systematically extended into the distal part of the lesser trochanter (Fig. 3). By contrast, in all *Pan*, 5/6 *Gorilla* and in the *Pongo* individual where it was unambiguously expressed, the distal end of the CF was typically confined to the proximal half of the lesser trochanter compartment, or occasionally near its middle portion. However, a typically human-like condition was found in one female *Gorilla*, whose distal extension was deep within the lesser trochanter (Fig. 3a; SOM Fig. S5).

Quantitative analyses revealed that humans had the absolutely greatest PT MaxLength, CF MaxLength, and CF MaxHeight (Fig. 5; Table 1). However, for PT MaxLength and CF MaxLength, *Gorilla* showed the greatest range of variation and also had the highest individual values. For all three variables, the differences between humans and *Pan* were statistically significant, while humans and *Gorilla* differed significantly only in CF MaxHeight (Fig. 5; Table 1; SOM Table S3). *Pan* and *Gorilla* also differed significantly only in CF MaxHeight (Fig. 5; Table 1; SOM Table S3). Relative to body size, humans had significantly larger PT MaxLength and CF MaxLength compared with *Gorilla*, and significantly higher CF MaxHeight compared with *Pan* and *Gorilla* (Fig. 5; Table 1; SOM Table S3). The *Pongo* specimen values were closer to those of *Gorilla* or intermediate between *Pan* and *Gorilla* (Fig. 5; Table 1). Calcar femoral root width was absolutely larger in *Gorilla* (Fig. 2c) and narrower in the captive *Pongo* individual, the

latter falling below the ranges of the three other taxa. However, human and great apes overlapped in both absolute and standardized values, with humans and *Gorilla* showing the greatest degree of overlap (SOM Table S4).

Spearman's correlation results revealed that PT MaxLength, CF MaxLength, CF MaxHeight, and CF root width were uncorrelated with CBT when controlling for body mass (SOM Fig.S3; SOM Tables S5 and S6). The distance between the periosteal surface and the most internal point of the CF (PT MaxLength), CF MaxLength, and CF MaxHeight were also uncorrelated with estimated body mass (SOM Table S7) in extant humans, *Pan*, and *Gorilla*. There was, however, a significant positive correlation between PT MaxLength and CBT, which is not surprising given that this measurement includes the cortical thickness (SOM Table S6).

3.3. Calcar femorale occurrence in the fossil hominid sample

The CF was present in five of the six specimens comprising our fossil sample: RUD 234 (*Rudapithecus*), StW 99 and 367 (*A. africanus*), and KNM-ER 738 and 1465 (likely *P. boisei*; Fig. 6). Conversely, we observed no trace of a CF on the endosteal contour of SK 97 (*P. robustus*), although possible strengthening of the trabeculae projecting towards the greater trochanter could not be confidently ascertained because of the incomplete preservation in this specimen (Fig. 6; SOM Fig. S6). Due to preservation quality, 3D rendering of the CF was possible only in RUD 234 and KNM-ER 738 (Fig. 7).

3.4. Comparison of the calcar femorale between the extant and fossil samples

None of the fossils showed distinct evidence of a bony reinforcement at the lateral margin of the lesser trochanter comparable to that found in some *Pan* and *Gorilla* specimens, and in the *Pongo* individual displaying the CF (Fig. 3; SOM Fig. S4).

RUD 234 showed a well-developed CF (Figs. 6 and 7), similar in structure to some *Pan* (Fig. 3; SOM Fig. S3) but extended more transversely. Indeed, CF MaxLength in RUD 234 slightly exceeded that of the CF in *Pongo* and fell within the upper end of the interquartile range of the *Gorilla* sample, outside of the range above *Pan*, and in the lower range (higher than the minimum value) of humans (Fig. 5; Table 2). RUD 234 also had a longer CF MaxLength relative to the other fossils. RUD 234 CF MaxHeight was found in the upper range (lower than the maximum value) of *Pan*, and was in the lower range of *Gorilla*, and lower than *Pongo* as well as the other three fossils for which CF MaxHeight could be assessed (Fig. 5; Table 2).

StW 99 and StW 367 (*A. africanus*) both displayed a short CF MaxLength, most comparable to that of *Pan*; StW 99 fell below the 25th percentile of *Pan* and in the lower end of the interquartile range of *Gorilla* while StW 367 fell below the 25th percentile of *Pan* and *Gorilla* (Fig. 5; Table 2). For CF MaxHeight, StW 99 fell well within the upper end of the range of variation of *Gorilla* and the lower range of extant humans, but well above the range of variation found in *Pan* (Fig. 5; Table 2). The distal end of the CF in StW 99 was not confined within the proximal portion of the lesser trochanter but extended at least to its mid portion, as seen in humans.

In KNM-ER 738, CF MaxLength fell in the upper end of the interquartile range of *Pan* and lower end of the interquartile range of *Gorilla*, lower than the minimum value of extant humans (Fig. 5; Table 2). Calcar femorale MaxLength in KNM-ER 1465 is slightly longer than in KNM-ER 738, falling in the lower end of the interquartile range of *Gorilla* near the median value and at the 75th percentile of *Pan*, in the lower range of variation of extant humans (Fig. 5; Table 2). In

KNM-ER 738, CF MaxHeight fell within the lower range of variation for *Gorilla* and in the upper range for *Pan* (Fig. 5; Table 2). In this specimen, the CF reached the upper region of the lesser trochanter (Fig. 7), while in KNM-ER 1465 the CF was longer and extended more distally (Fig. 5; Table 2), similar to the condition found in StW 99.

In the five fossils displaying a CF, the CF root width was broad, particularly in the two *A. africanus* specimens, overlapping with the *Pan* and *Gorilla* and broader than that of our extant human sample (SOM Fig. S7).

4. Discussion and conclusions

This study explored the occurrence and, when present, 3D morphology of the CF in extant humans, great apes, *Papio*, and a sample of fossil hominids. We found that a CF is most commonly found in extant humans, but that there was substantial variation in CF occurrence and morphology across our sample, including within humans. These results add to previous studies that have called into question the functional significance of the CF.

4.1. Extant hominoids

Based on previous studies (Farkas et al., 1948; White, 1984; Reed et al., 1993; Grine et al., 1995: Kuperavage et al., 2018; Hammer, 2019), we predicted that, compared to great apes, the CF in humans would be expressed more frequently, and absolutely and relatively longer and more vertically extended, with a thicker root width. However, only its higher frequency (90% in humans vs. 60–65% in the *Pan* and *Gorilla* samples) and absolute and standardized average height of the CF clearly distinguish humans from other extant hominids. Indeed, contrary to our expectation, no

other quantitative CF variables measured in our study unambiguously discriminate between humans and great apes. Although our hominoid sample sizes were relatively small (n = 9–10) and larger samples may provide greater discrimination in CF morphology across taxa, it is notable that we nonetheless found substantial intraspecific variability in each hominoid taxon, including humans. In addition, the extent to which geometric differences in the proximal femur (i.e., neck shaft angle, superoinferior length of the greater trochanter, projection of the head relative to the greater trochanter; Harmon, 2007) across hominoids contribute to the distal extension of the CF in humans requires further investigation.

Whatever the cause(s) responsible for the expression of a spur of vertically and transversely thickened bone within the femoral neck, and whatever its functional significance (Farkas et al., 1948; Li and Aspden, 1997, 1998; Gao et al., 1999; Wang et al., 2005; Zhang et al., 2009; Hammer, 2019), our results make clear that presence vs. absence of a CF does not distinguish humans from great apes. As noted above, variation in the expression of the CF was also observed in our extant human sample (e.g., one individual did not show any trace of a CF), supporting previous studies identifying variability in shape and proportions of the CF in humans (e.g., Thompson, 1907; Glinkowki and Ciszek, 1989; Le Corroller et al., 2011; Kuperavage et al., 2018).

Additional comparative study of the ontogeny of CF expression in humans and extant great apes would provide much-needed information on when the CF first appears during growth and patterns of age-related strengthening, notably with respect to the onset of independent locomotion. This approach which has already provided valuable information when applied to the endostructural organization of the proximal femur (e.g., Ryan and Krovitz, 2006; Raichlen et al., 2015; Milovanovic et al., 2017; Tsegai et al., 2018b). In this context, investigation of the role of a growing iliopsoas tendon in the ontogeny of CF expression and morphology (Cunningham et al.,

2016) should be particularly informative given that in humans, the CF is thought to be related to the load created by the insertion of this musculotendinous complex (Tatu et al., 2002) on the lesser trochanter (Cunningham et al., 2016), which has a fulcrum at the femoral head to increase its moment arm (Hogervorst and Vereecke, 2015).

Our second prediction was that extant great ape taxa would show a similar degree of CF occurrence given their shared high degree of hip joint mobility (Isler and Thorpe, 2003; Hammond, 2013; Finestone et al., 2018) and their similar patterns of cortical and trabecular bone distribution in the proximal femur, which suggest similar loading conditions at the hip joint (Rafferty, 1998; Ryan and Shaw, 2012; Georgiou et al., 2019; Pina et al., 2019). This prediction was partially supported by our results. Our study confirmed the frequent presence of a CF in *Pan* (Kuperavage et al., 2018) and, for the first time, also showed that a CF commonly occurs in *Gorilla* (cf. Crompton et al., 2021). However, a CF was only been identified in one captive *Pongo* (while it is absent in another captive individual from the same zoo).

Within the three great ape taxa we also expected to detect a comparable shape, extension into the lesser trochanter, absolute and relative vertical length, height and root width of the CF. This prediction is not supported as we found high degree of variation between the African apes. Compared to the more common human condition, *Pan* shows a less proximodistally developed CF. Kuperavage et al. (2018) also found a degree of vertical extension comparable to the human pattern in two of seven *Pan* bearing a CF. However, one *Gorilla* included in our sample shows a human-like CF with a distal end that extends to the middle-lower part of the lesser trochanter. Interestingly, compared to *Pan*, the *Gorilla* sample is more similar to the human condition in PT MaxLength and CF MaxLength. However, when standardized by body mass, humans and *Pan* overlap in CF transverse length, while CF transverse length in *Gorilla* is absolutely shorter

compared to *Pan* and *Pongo*. In all cases, the degree of CF transverse extension is uncorrelated with both cortical bone thickness variation at the lesser trochanter cross-sectional level and with body mass. Finally, we find a similar extent of variation in *Pan* (see also Kuperavage et al., 2018) and in *Gorilla*.

The variation in CF morphology observed between African apes and *Pongo* might reflect documented differences in climbing frequency and kinematics. Specifically, *Pan* and *Gorilla* vertically climb and descend less frequently (Hunt, 1991; Doran, 1996; Thorpe and Crompton, 2006) and have lower range of hip extension, abduction and external rotation (Isler, 2005; Hammond, 2013, 2014) compared with that of *Pongo*. In addition, although the cortical and trabecular distribution patterns are generally similar across great apes at the proximal femur (Ryan and Shaw, 2012; Georgiou et al., 2019, 2020), *Pongo* is distinct in having a lower trabecular bone density in the femoral head (Georgiou et al., 2019), suggesting subtle differences in loading magnitude or direction at the hip joint, which may explain variation in CF expression between the African apes and *Pongo*. If the lower frequency of a CF in *Pongo* is related to its arboreal suspensory specializations, then we would expect a similar condition in hylobatids given their shared hip range of motion related to their suspensory behaviors (Hammond, 2013, 2014). In a preliminary assessment of two *Hylobates lar* we found no evidence of a CF (SOM Fig. S8), but further examination with a larger sample is needed to confirm this finding. The possible influence of captivity-related mechanical/environmental constraints on CF expression in extant great apes is currently unknown but the variable presence of a CF in captive *Pongo* coupled with the complete absence in wild *Pongo* individuals, as shown in this study, emphasizes the need for further investigation.

Finally, our prediction that none of the *Papio* specimens included in our sample would show evidence of a CF was supported. This result is consistent with results previously reported for rhesus macaques (Glinkowski and Ciszek, 1989). . In general, future research examining CF presence and patterns of variation in larger samples of extant apes, with special attention to the degree of expression of this feature between sister taxa that vary in the frequency of different locomotor behaviors (e.g., *P. troglodytes* vs. *Pan paniscus*; *G. gorilla* vs. *Gorilla beringei*; Hunt, 1991; Crompton et al., 2010) may shed light on the variation in CF expression and its potential functional significance. Moreover, although we did not quantitatively evaluate sex differences in the CF in this study, future investigations should also examine the possible influence of sexual dimorphism on CF expression.

4.2 Fossil hominins and Rudapithecus

We predicted that the fossil hominins (*Australopithecus* and *Paranthropus*) in our sample would display a CF morphology more similar to extant humans given that they are all considered habitual bipeds when terrestrial. We also expected the orthograde suspensory *Rudapithecus* to show a CF morphology more similar to that of the great apes. Both predictions were generally supported, but with some notable exceptions. The results of our high-resolution analyses of the occurrence and 3D shape variation of the CF in a selected sample of hominid representatives (*Rudapithecus*, *Australopithecus*, *Paranthropus*) are in line with our results for our extant hominid sample. This is also the case for evidence provided by previous studies of fossil hominin femora (White, 1984; Grine et al., 1995; Kuperavage et al., 2018). Indeed, although not all CF variables could be assessed due to variable preservation, the CF was present in all investigated fossil hominid specimens except SK 97 (*P. robustus*). However, CF morphology (i.e., shape, location, extension

within the lesser trochanter, absolute horizontal length, absolute vertical height, and root width) in fossil hominids varied to an extent comparable to that observed in our extant hominid sample and the CF dimensions do not always fall within the human range of variation. Specifically, among the fossil hominins, a human-like CF vertical extension is found in *A. africanus* StW 99 and *P. boisei* KNM-ER 1465, with both specimens showing a CF confined within the proximal portion of the lesser trochanter, while other fossils have a shorter distal extension.

A previous study has reported the presence of a CF in the two partial femora of *Orrorin*, BAR 1002'00 and 1003'00, but only the latter, less heavily mineralized specimen could be assessed quantitatively (Kuperavage et al., 2018). Axial virtual cross sections obtained from a medical CT scan showed the presence of a distinct CF. However, the reported absolute length of the *Orrorin* CF (1.58 cm; Kuperavage et al., 2018) is most similar to the mean values we have documented in humans and *Gorilla*. Moreover, its observed distal extension to the middle of the lesser trochanter (Kuperavage et al., 2018) is intermediate between the average conditions we measured in *Pan* and humans and, most similar to the morphology displayed in a female *Gorilla* (SOM Fig. S5) and a captive male *Pongo* (Fig. 3).

The variation in CF occurrence and expression documented in the fossil hominin sample here, in combination with previous studies (i.e., *Orrorin*, *Australopithecus*, Middle Pleistocene *Homo*), may reflect variation in the biomechanics and/or frequency of bipedal (or climbing) locomotion these hominin taxa. Alternatively, this variation, including the notable absence of a CF in SK 97, may simply represent 'normal' variation in CF occurrence and expression that has been documented here and in previous studies (Kuperavage et al., 2018) among humans and other great apes, further emphasizing that presence/absence of a CF is not a reliable indicator of bipedalism. A comprehensive analysis of the degree of development of the CF in hominin taxa that also

combines cortical thickness topographic distribution and trabecular structural organization at the proximal femoral end (e.g., Ohman et al., 1997; Ruff and Higgins, 2013; Kivell, 2016; Ruff et al., 2016; Cazenave et al., 2019, 2021; Ryan et al., 2018; Georgiou et al., 2020) may reveal whether CF variation reflects individual differences in mechanical strength across the different compartments, and therefoe, individual differences in the loading environment of the hip joint.

Importantly, we also detected a *Pan*-like CF in *Rudapithecus* RUD 234, but more transversely extended, as observed in *Gorilla*. This finding is especially interesting given that short-distance bipedal walking and stance behaviors are variably displayed by all great apes, including occasionally by *Pongo* when moving on flexible branches (Thorpe et al., 2007; Crompton, et al., 2010). In addition, the external postcranial morphology of the stem hominid dryopithecin *Danuvius guggenmosei* (Böhme et al., 2019) has been interpreted as reflecting habitual bipedal postures (but see Williams et al., 2020). Thus, the potential that *Rudapithecus* may have engaged in similar bipedal postures than great apes cannot be excluded, although bipedalism is a minor component of the *Pan* locomotor repertoire (0.4–8.0% of locomotor time; Hunt, 1991). The results of our study thus suggest that CF morphology in extant great apes and *Rudapithecus* may represent a bone functional adaptation to different orthograde locomotor behaviors likely related to a more extended hip joint such as during vertical climbing or extended-limb clambering (Isler, 2005; Böhme et al., 2019), rather than bipedalism specifically.

Potentially valuable information about the functional link between the CF and bipedalism could derive from the analysis of the proximal femora of Sansuke, an adult *Macaca fuscata* that regularly engaged for eight years in bipedal performance (Nakatsukasa et al., 1995). The femora of this individual have not yet been investigated for the presence of a CF, but previous research has shown that cortical bone thickness distribution and trabecular organization within the innominate, the

femur, and the proximal tibia show distinct adaptive responses to the more compressive loads imposed by bipedal locomotion (Nakatsukasa and Hayama, 2003; Volpato et al., 2008; Mazurier et al., 2010). If the CF, or at least a CF-like structure plays an active role in transferring loads incurred during bipedal gait from the femoral head through the neck to the shaft (see review in Hammer, 2019), Sansuke's proximal femora should show at least traces of a cortico-trabecular strengthening extended across this region compared to wild *M. fuscata* individuals.

In conclusion, this study demonstrated that humans are distinguished from extant great apes in the more frequent occurrence of a CF, and a CF that is distinct in its greater proximodistal extension to within the lesser trochanter. However, an increasing body of comparative evidence from extant and extinct hominid taxa shows that the CF is a highly variable, possibly ecophenotypic (i.e, modified during life by environmental factors) structure, even in humans. As already suggested by its previous identification in some *Pan* femora (Kuperavage et al., 2018), the presence of a CF-like structure and even human-like CF in some great apes makes clear that this feature cannot be reliably considered as a 'magic trait' (sensu Stern and Susman, 1991) to identify habitual bipedal locomotion in hominins. In light of our results, several future investigations have been suggested that may elucidate the possible functional influence on the degree of expression of the CF. Higher resolution imaging and quantitative assessment of the CF in *Orrorin* BAR 1003'00, and the analysis of the partial femora representing the late Miocene taxa *Danuvius* (Böhme et al., 2019) and *Sahelanthropus* (Macchiarelli et al., 2020) would further contribute the understanding of the evolutionary history of this trait.

Acknowledgments

For access to fossil and comparative materials, we are grateful to the curatorial staff of the Ditsong National Museum of Natural History, Pretoria; the Evolutionary Studies Institute at the University of the Witwatersrand, Johannesburg; the Mining and Geological Survey of Hungary (MBFSZ); the Institut Català de Paleontologia Miquel Crusafont, Sabadell; the McGregor Museum of Kimberley; the Mining and Geological Survey of Hungary, Budapest; the Museum National d'Histoire Naturelle (MNHN), Paris; the National Museums of Kenya (KNM), Nairobi; the Pretoria Bone Collection at the Department of Anatomy of the University of Pretoria. We acknowledge C. Boesch for access to the *Pan* sample at the Max Planck Institute for Evolutionary Anthropology (MPI), Leipzig; L. Hutten to the baboon sample from the University of Cape Town; I. Livne to the *Gorilla* sample of the Powell-Cotton Museum; A. Van Heteren to the *Pongo* sample of the Zoologische Staatssammlung München. For the extant human comparative sample, ethical clearance was obtained from the Faculty of Health Sciences Research Ethics committee of the University of Pretoria (ref. no. 39/ 2016). We especially acknowledge J.-J. Hublin (Leipzig), E. L'Abbé (Pretoria), D. Morris (Kimberley), A. Oettlé (Pretoria), F. Thackeray (Johannesburg), K. Palotás (Budapest) and B. Zipfel (Johannesburg). We thank M. Bellato for scanning the *Pan* sample at the AST-RX Plateau d'Accès Scientifique à la Tomographie à Rayons X of the UMS 2700 2AD CNRS-MNHN, Paris (data kindly shared by R. Macchiarelli). We thank F. de Beer (Pelindaba), J. Hoffman (Pelindaba), L. Bam (Pelindaba), K. Jakata (Johannesburg), K. Smithson (University of Cambridge), and D. Plotzki (MPI) for µCT scanning at Necsa, Wits, Cambridge and MPIEVA, respectively, and the staff of industrial-CT YXLON Compact at the Human Evolution Lab. (LEB) at the Universidad de Burgos. For availability to run independent measures for interobserver error assessment, we thank A. Bardo (Canterbury). For discussion, we thank A. Beaudet (Cambridge), C. Dunmore (Canterbury), S. Syeda (Canterbury), C. Theye (Pretoria), Z.

Tsegai (Leipzig). Finally, we are grateful to Andrea Taylor, the Associate Editor, and to three anonymous reviewers for constructive critique that considerably improved this manuscript. We acknowledge the DST-NRF for financial support (Grant # UID23456) to establish the MIXRAD microfocus X-ray tomography facility at Necsa. M.C. is funded by the Fyssen Foundation. M.P. is funded by European Commission under the Marie Skłodowska-Curie Individual Fellowship Programme (H2020-MSCA-IF-2018-837966). This project has received funding from the European Research Council (grant agreement No. 819960).

References

Aiello, L., Dean, C., 1990. An Introduction to Human Evolutionary Anatomy. Academic Press, New York.

Adam, F., Hammer, D.S., Pape, D., Kohn, D., 2001. The internal calcar septum (femoral thigh spur) in computed tomography and conventional radiography. Skelet. Radiol. 30, 77-83.

Almécija, S., Hammond, A.S., Thompson, N.E., Pugh, K.D., Moyà-Solà, S., Alba, D.M., 2021. Fossil apes and human evolution. Science 372, eabb4363.

Barak, M.M., Lieberman, D.E., Hublin, J.-J., 2011. A Wolff in sheep's clothing: Trabecular bone adaptation in response to changes in joint loading orientation. Bone 49, 1141-1151.

Begun, D.R., 1993. New catarrhine phalanges from Rudabánya (Northeastern Hungary) and the problem of parallelism and convergence in hominoid postcranial morphology. J. Hum. Evol. 24, 373-402.

Begun, D.R., Nargolwalla, M.C., Kordos, L., 2012. European Miocene hominids and the origin of the African ape and human clade. Evol. Anthropol. 21, 10-23.

Biewener, A.A., Fazzalari, N.L., Konieczynski, D.D., Baudinette, R.V., 1996. Adaptive changes in trabecular architecture in relation to functional strain patterns and disuse. Bone 19, 1-8.

Bigelow, H.J., 1875. The true neck of the femur: Its structure and pathology. Boston Med. Surg. J. 92, 1-5.

Böhme, M., Spassov, N., Fuss, J., Tröscher, A., Deane, A.S., Prieto, J., Kirscher, U., Lechner, T., Begun, D.R., 2019. A new Miocene ape and locomotion in the ancestor of great apes and humans. Nature 575, 489-493.

Bonewald, L.F., Johnson, M.L., 2008. Osteocytes, mechanosensing and Wnt signaling. Bone 42, 606-615.

Buie, H.R., Campbell, G.M., Klinck, R.J., MacNeil, J.A., Boyd, S.K., 2007. Automatic segmentation of cortical and trabecular compartments based on a dual threshold technique for in vivo micro-CT bone analysis. Bone 41, 505-515.

Burgess, M.L., McFarlin, S.C., Mudakikwa, A., Cranfield, M.R., Ruff, C.B., 2018. Body mass estimation in hominoids: Age and locomotor effects. J. Hum. Evol. 115, 36-46.

Carlson, K.J., Judex, S., 2007. Increased non-linear locomotion alters diaphyseal bone shape. J. Exp. Biol. 210, 3117-3125.

Cazenave, M., Braga, J., Oettlé, A., Pickering, T.R., Heaton, J.L., Nakatsukasa, M., Thackeray J.F., de Beer, F., Hoffman, J., Dumoncel, J., Macchiarelli, R., 2019. Cortical bone distribution in the femoral neck of *Paranthropus robustus*. J. Hum. Evol. 135, 102666.

Cazenave, J., Oettle, A., Pickering, T.R., Heaton, J.L., Nakatsukasa, M., Thackeray, J.F., de Beer, F., Hoffman, J., Dumoncel, J., Macchiarelli, R., 2021. Trabecular organization of the proximal femur in *Paranthropus robustus*: Implications for the assessment of its hip joint loading conditions. J. Hum. Evol. 153, 102964.

Chang, G., Pakin, S.K., Schweitzer, M.E., Saha, P.K., Regatte, R.R., 2008. Adaptations in trabecular bone microarchitecture in Olympic athletes determined by 7T MRI. J. Magn. Res. Imag. 27, 1089-1095.

Cresswell, E.N., Goff, M.G., Nguyen, T.M., Lee, W.X., Hernandez, C.J., 2015. Spatial relationships between bone formation and mechanical stress within cancellous bone. J. Biomech. 49, 222-228.

Crompton, R.H., Sellers, W.I., Thorpe, S.K.S., 2010. Arboreality terrestriality and bipedalism. Phil. Trans. Biol. Sci. 365, 3301-3314.

Crompton, R.H., McClymont, J., Elton, S., Thorpe, S., Sellers, W., Heaton, J., Pickering, T.R., Pataky, T., Carlson, K.J., Jashashvili, T., Beaudet, A., Bruxelles, L., Goh, E.,·Kuman, K., Clarke, R. (2021). StW 573 *Australopithecus prometheus*: Its significance for an australopith bauplan. Folia Primatol. 92, 243-275.

Cunningham, C.A., Black, S.M., 2009. Anticipating bipedalism: Trabecular organization in the newborn ilium. J. Anat. 214, 817-829.

Cunningham, C.A., Scheur, L., Black, S., 2016. Developmental Juvenile Osteology, 2nd ed. Academic Press, London.

Demissie, S., Dupuis, J., Cupples, L.A., Beck, T., Kiel, D.P., Karasik, D., 2007. Proximal hip geometry is linked to several chromosomal regions: Genome-wide linkage results from the Framingham Osteoporosis Study. Bone 40, 743-750.

Dixon, A.F., 1910. The architecture of the cancellous tissue forming the upper end of the femur. J. Anat. Physiol. 44, 223-230.

Doran, D.M., 1996. The comparative positional behavior of the African apes. In: McGrew, W., Nishida, T. (Eds.), Great Ape Societies. Cambridge University Press, Cambridge, pp. 213-224.

Estrada, K., Styrkarsdottir, U., Evangelou, E., Hsu, Y.H., Duncan, E.L., Ntzani, E.E., Oei, L., Albagha, O.M., Amin, N., Kemp, J.P., Koller, D.L., Li, G., Liu, C.T., Minster, R.L., Moayyeri, A., Vandenput, L., Willner, D., Xiao, S.M., Yerges-Armstrong, L.M., Zheng, H.F., Alonso, N., Eriksson, J., Kammerer, C.M., Kaptoge, S.K., Leo, P.J., Thorleifsson, G., Wilson, S.G., Wilson, J.F., Aalto, V., Alen, M., Aragaki, A.K., Aspelund, T., Center, J.R., Dailiana, Z., Duggan, D.J., Garcia, M., Garcia-Giralt, N., Giroux, S., Hallmans, G., Hocking, L.J., Husted, L.B., Jameson, K.A., Khusainova, R., Kim, G.S., Kooperberg, C., Koromila, T., Kruk, M., Laaksonen, M., Lacroix, A.Z., Lee, S.H., Leung, P.C., Lewis, J.R., Masi, L., Mencej-Bedrac, S., Nguyen, T.V., Nogues, X., Patel, M.S., Prezelj, J., Rose, L.M., Scollen, S., Siggeirsdottir, K., Smith, A.V., Svensson, O., Trompet, S., Trummer, O., van Schoor, N.M., Woo, J., Zhu, K., Balcells, S., Brandi, M.L., Buckley, B.M., Cheng, S., Christiansen, C., Cooper, C., Dedoussis, G., Ford, I., Frost, M., Goltzman, D., González-Macías, J., Kähönen, M., Karlsson, M., Khusnutdinova, E., Koh, J.M., Kollia, P., Langdahl, B.L., Leslie, W.D., Lips, P., Ljunggren, Ö., Lorenc, R.S., Marc, J., Mellström, D., Obermayer- Pietsch, B., Olmos, J.M., Pettersson-Kymmer, U., Reid, D.M., Riancho, J.A., Ridker, P.M., Rousseau, F., Slagboom, P.E., Tang, N.L., Urreizti, R., Van Hul, W., Viikari, J., Zarrabeitia, M.T., Aulchenko, Y.S., Grundberg, E., H errera, L., Ingvarsson, T., Johannsdottir, H., Kwan, T., Li, R., Luben, R., Medina-Gómez, C., Palsson, S.T., 866 Reppe, S., Rotter, J.I., Sigurdsson, G., van Meurs, J.B., Verlaan, D., Williams, F.M., Wood, A.R., Zhou, Y., Gautvik, K.M., Pastinen, T., Raychaudhuri, S., Cauley, J.A., Chasman, D.I., Clark, G.R., Cummings, S.R., Danoy, P., Dennison, E.M., Eastell, R., Eisman, J.A., Gudnason, V.,

Hofman, A., Jackson, R.D., Jones, G., Jukema, J.W., Khaw, K.T., Lehtimäki, T., Liu, Y., Lorentzon, M., McCloskey, E., Mitchell, B.D., Nandakumar, K., Nicholson, G.C., Oostra, B.A., Peacock, M., Pols, H.A., Prince, R.L., Raitakari, O., Reid, I.R., Robbins, J., Sambrook, P.N., Sham, P.C., Shuldiner, A.R., Tylavsky, F.A., van Duijn, C.M., Wareham, N.J., Cupples, L.A., Econs, M.J., Evans, D.M., Harris, T.B., Kung, A.W., Psaty, B.M., Reeve, J., Spector, T.D., Streeten, E.A., Zillikens, M.C., Thorsteinsdottir, U., Ohlsson, C., Karasik, D., Richards, J.B., Brown, M.A., Stefansson, K., Uitterlinden, A.G., Ralston, S.H., Ioannidis, J.P., Kiel, D.P., Rivadeneira, F., 2012. Genome-wide meta-analysis identifies 56 bone mineral density loci and reveals 14 loci associated with risk of fracture. Nat. Genet. 44, 491-501.

Fajardo, R.J., Müller, R., 2001. Three-dimensional analysis of nonhuman primate trabecular architecture using micro-computed tomography. Am. J. Phys. Anthropol. 115, 327-336.

Fajardo, R.J., Müller, R., Ketcham, R.A., Colbert, M., 2007. Nonhuman anthropoid primate femoral neck trabecular architecture and its relationship to locomotor mode. Anat. Rec. 290, 422-436.

Farkas, R.A., Wilson, M.J., Hayner, C., 1948. An anatomical study of the mechanics, pathology, and healing of fracture of the femoral neck. J. Bone Joint Surg. Am. 30, 53-59.

Finestone, E.M., Brown, M.H., Ross, S.R., Pontzer, 891 H., 2018. Great ape walking kinematics: Implications for hominoid evolution. Am. J. Phys. Anthropol. 166, 43-55.

Gao, L.J., Qiu, S.J., Dai, K.R., 1999. The microstructure and three dimensional structure of calcar femorale and the mechanics of its load capacity (Chin). Zhonghua Gu Ke Za Zhi 19, 109-112.

Garden, R.S., 1961. The structure and function of the proximal end of the femur. J. Bone Joint Surg. Br 43, 576-589.

Georgiou, L., Kivell, T.L., Pahr, D.H., Buck, L.T., Skinner, M.M., 2019. Trabecular architecture of the great ape and human femoral head. J. Anat.234, 679-693.

Glinkowski, W., Ciszek, B., 1989. The topographic and comparative study of the calcar femorale. Folia Morphol. 48, 183-191.

Gocha, T.P., Agnew, A.M., 2016. Spatial variation in osteon population density at the human femoral midshaft: Histomorphometric adaptations to habitual load environment. J. Anat. 228, 733-745.

Griffin, J.B., 1982. The calcar femorale redefined. Clin. Orthop. Relat. Res. 164, 211-214.

Grine, F.E., Jungers, W.L., Tobias, P.V., Pearson, O.M., 1995. Fossil *Homo* femur from Berg Aukas, northern Namibia. Am. J. Phys. Anthropol. 97, 151-185.

Guldberg, R.E., Caldwell, N.J., Guo, X.E., 1997. Mechanical stimulation of tissue repair in the hydraulic bone chamber. J. Bone Min. Res. 12, 1295-1302.

Hammer, A., 2010. The structure of the femoral neck: A physical dissection with emphasis on the internal trabecular system. Ann. Anat. 192, 168-177.

Hammer, A., 2019. The calcar femorale: A new perspective. J. Orthop. Surg. Res. 27, 1-9.

Hammond, A.S., 2013. 3D analysis of hip joint mobility and the evolution of locomotor abilities in Miocene hominoids. Ph.D. Dissertation, University of Missouri-Columbia.

Hammond, A.S., 2014. In vivo baseline measurements of hip joint range of motion in suspensory and nonsuspensory anthropoids. Am. J. Phys. Antropol. 153, 417-434.

Harmon, E.H., 2007. The shape of the hominoid proximal femur: A geometric morphometric analysis. J. Anat. 210, 170-185.

Harmon, E., 2009. Size and shape variation in the proximal femur of *Australopithecus africanus*. J. Hum. Evol. 56, 551-559.

Harty, M., 1957. The calcar femorale and the femoral neck. J. Bone Joint Surg. 39A, 625-630.

Havill, L.M., Allen, M.R., Bredbenner, T.L., Burr, D.B., Nicolella, D.P., Turner, C.H., Warren, D.M., Mahaney, M.C., 2010. Heritability of lumbar trabecular bone mechanical properties in baboons. Bone 46, 835-840.

Havill, L.M., Mahaney, M.C., Binkley, T.L., Specker, B.L., 2007. Effects of genes, sex, age, and activity on BMC, bone size, and areal and volumetric BMD. J. Bone Min. Res. 22, 737-746.

Hogervorst, T., Vereecke, E.E., 2015. Evolution of the human hip. Part 2: Muscling the double extension. J. Hip Pres. Surg. 2, 3-14.

Hou, R., Cole, S.A., Graff, M., Haack, K., Laston, S., Comuzzie, A.G., Mehta, N.R., Ryan K., Cousminer D.L., Zemel, B.S., Grant S.F.A., Mitchell, B.D., Shypailo, R.J., Gourlay, M.L., North, K.E., Butte, N.F., Grant, S.F., 2020. Genetic variants affecting bone mineral density and bone mineral content at multiple skeletal sites in Hispanic children. Bone 132, 115175.

Hunt, K.D., 1991. Positional behavior in the Hominoidea. Int. J. Primatol. 12, 95-118.

Hunt, K.D., Cant, J.G.H., Gebo, D.L., Rose, M.D., Walker, S.E., Youlatos, D., 1996. Standardized descriptions of primate locomotor and postural modes. Primates 37, 363-387.

Isler, K., Thorpe, S.K., 2003. Gait parameters in vertical climbing of captive, rehabilitant and wild Sumatran orang-utans (*Pongo pygmaeus abelii*). J. Exp. Biol. 206, 4081-4096.

Isler, K., 2005. 3D-Kinematics of vertical climbing in hominoids. Am. J. Phys. Antropol. 126, 66-81.

Judex, S., Garman, R., Squire, M., Leah-Rae, D., Rubin, C., 2004. Genetically based influences on the site-specific regulation of trabecular and cortical bone morphology. J. Bone Min. Res. 19, 600-606.

Kapandji, A.I., 2011. The Physiology of the Joints. Vol. 2. The Lower Limb, 6th ed. Elsevier, Edinburgh.

Kivell, T.L., Begun, D.R., 2009. New primate carpal bones from Rudabánya (late Miocene, Hungary): Taxonomic and functional implications. J. Hum. Evol. 57, 697-709.

Kuperavage, A., 2009. Inferences concerning bipedal locomotion from the internal structure of the BAR 1002’00 and BAR 1003’00 femoral fragments. Ph.D. Dissertation, Penn State University.

Kuperavage, A., Pokrajac, D., Chavanaves, S., Eckhardt, R.B., 2018. Earliest known hominin calcar femorale in *Orrorin tugenensis* provides further internal anatomical evidence for origin of human bipedal locomotion. Anat. Rec. 30, 1834-1839.

Lanyon, L.E., 1973. Analysis of surface bone strain in the sheep during normal locomotion. J. Biomech. 6, 41-49.

Le Corroller, T., Dediu, M., Pauly, V., Pirro, N., Chabrand, P., Champsaur, P., 2011. The femoral calcar: A computed tomography anatomical study. Clin. Anat. 24, 886-892.

Levangie, P.K., Norkin, C.C., 2011. Joint Structure and Function: A Comprehensive Analysis. F.A. Davis, Philadelphia.

Li, B., Aspden, R.M., 1997. Material properties of bone from the femoral neck and calcar femorale of patients with osteoporosis or osteoarthritis. Osteopor. Int. 7, 450-456.

Li, B., Aspden, R.M., 1998. A comparison of the stiffness, density and composition of bone from the calcar femorale and the femoral cortex. J. Mat. Sci. Mater. Med. 9, 661-666.

Lovejoy, C.O., 1988. Evolution of human walking. Sci. Am. 259, 118-125.

Lovejoy, C.O., 2005. The natural history of human gait and posture. Part 2. Hip and thigh. Gait & Posture 21, 113-124.

Lovejoy, C.O., Cohn, M.J., White, T.D., 1999. Morphological analysis of the mammalian postcranium: A developmental perspective. Proc. Natl. Acad. Sci. USA 96, 13247-13252.

Lovejoy, C.O., Meindl, R.S., Ohman, J.C., Heiple, K.G., White, T.D., 2002. The Maka femur and its bearing on the antiquity of human walking: Applying contemporary concepts of morphogenesis to the human fossil record. Am. J. Phys. Anthropol. 119, 97-133.

Macchiarelli, R., Bergeret-Medina, A., Marchi, D., Wood, B., 2020. Nature and relationships of *Sahelanthropus tchadensis*. J. Hum. Evol. 149, 102898.

MacLatchy, L., Müller, R., 2002. A comparison of the femoral head and neck trabecular architecture of *Galago* and *Perodicticus* using micro-computed tomography (microCT). J. Hum. Evol. 43, 89-105.

Mazurier, A., Nakatsukasa, M., Macchiarelli, R., 2010. The inner structural variation of the primate tibial plateau characterized by high-resolution microtomography. Implications for the reconstruction of fossil locomotor behaviours. C. R. Palevol 9, 349-359.

Medina-Gomez, C., Kemp, J.P., Trajanoska, K., Luan, J.A., Chesi, A., Ahluwalia, T.S., Mook-Kanamori, D.O., Ham, A., Hartwig, F.P., Evans, D.S., Joro, R., Nedeljkovic, I., Zheng, H.F., Zhu, K., Atalay, M., Liu, C.T., Nethander, M., Broer, L., Porleifsson, G., Mullin, B.H., Handelman, S.K., Nalls, M.A., Jessen, L.E., Heppe, D.H.M., Richards, J.B., Wang, C., Chawes, B., Schraut, K.E., Amin, N., Wareham, N., Karasik, D., Van der Velde, N., Ikram, M.A., Zemel, B.S., Zhou, Y., Carlsson, 1011 C.J., Liu, Y., McGuigan, F.E., Boer, C.G.,Bønnelykke, K., Ralston, S.H., Robbins, J.A., Walsh, J.P., Zillikens, M.C., Langenberg, C., Li-Gao, R., Williams, F.M.K., Harris, T.B., Akesson, K., Jackson, R.D., Sigurdsson, G., den Heijer, M., van der Eerden, B.C.J., van de Peppel, J., Spector, T.D., Pennell, C., Horta, B.L., Felix, J.F., Zhao, J.H., Wilson, S.G., de Mutsert, R., Bisgaard, H., Styrkársdóttir, U., Jaddoe, V.W., Orwoll, E., Lakka, T.A., Scott, R., Grant, S.F.A., Lorentzon, M., van Duijn, C.M., Wilson, J.F., Stefansson, K., Psaty, B.M., Kiel, D.P., Ohlsson, C., Ntzani, E., van Wijnen, A.J., Forgetta, V., Ghanbari, M., Logan, J.G., Williams, G.R., Bassett, J.H.D., Croucher, P.I., Evangelou, E., Uitterlinden, A.G., Ackert-Bicknell, C.L., Tobias, J.H., Evans, D.M., Rivadeneira, F., 2018.

Life-course genome-wide association study meta-analysis of total body BMD and assessment of age-specific effects. Am. J. Hum. Genet. 102, 88-102.

Merkel, F., 1874. Betrachtungen über das Os femoris. Vircows Arch. f. Pathol. Anat. 59, 237-256.

Miller, Z., Fuchs, M.B., Arcan, M., 2002. Trabecular bone adaptation with an orthotropic material model. J. Biomech. 35, 247-256.

Milovanovic, P., Djonic, D., Hahn, M., Amling, M., Busse, B., Djuric, M., 2017. Region dependent patterns of trabecular bone growth in the human proximal femur: A study of 3D bone microarchitecture from early postnatal to late childhood period. Am. J. Phys. Anthropol. 164, 281-291.

Mittra, E., Rubin, C., Qin, Y.X., 2005. Interrelationship of trabecular mechanical and microstructural properties in sheep trabecular bone. J. Biomech. 38, 1229-1237.

Morbeck, M.E., 1983. Miocene hominoid discoveries from Rudabánya. In: Ciochon, R.L., Corruccini, R.S. (Eds.), New Interpretations of Ape and Human Ancestry. Springer, Boston, pp. 369-404.

Mori, T., Okimoto, N., Sakai, A., Okazaki, Y., Nakura, N., Notomi, T., Nakamura, T., 2003. Climbing exercise increases bone mass and trabecular bone turnover through transient

regulation of marrow osteogenic 1035 and osteoclastogenic potentials in mice. J. Bone Min. Res. 18, 2002-2009.

Nakatsukasa, M., Hayama, S., 2003. Skeletal response to bipedalism in macaques, with emphasis on cortical bone distribution of the femur. Cour. Forsch-Inst. Sencken. 243, 35-45.

Nakatsukasa, M., Hayama, S., Preuschoft, H., 1995. Postcranial skeleton of a macaque trained for bipedal standing and walking and implications for functional adaptation. Folia Primatol. 64, 1-29.

Newell, R.L.M., 1997. The calcar femorale: A tale of historical neglect. Clin. Anat. 10, 27-33.

Ohman, J.C., 1993. Cross sectional geometric properties from biplanar radiographs and computed tomography: functional application to the humerus and femur in Hominoids. Ph.D. Dissertation, Kent State University.

Ohman, J.C., Krochta, T.J., Lovejoy, C.O., Mensforth, R.P., Latimer, B., 1997. Cortical bone distribution in the femoral neck of hominoids: Implications for the locomotion of *Australopithecus afarensis*. Am. J. Phys. Anthropol. 104, 117-131.

O'Neill, M.C., Dobson, S.D., 2008. The degree and pattern of phylogenetic signal in primate long-bone structure. J. Hum. Evol. 54, 309-322.

Pickering, T.R., Heaton, J.L., Clarke, R.J., Stratford, D., Heile, A.J., 2021. Hominin lower limb bones from Sterkfontein Caves, South Africa (1998-2003 excavations). South Afr. J. Sci. 117, 1-10.

Pickford, M., Senut, B., Gommery, D., Treil, J., 2002. Bipedalism in *Orrorin tugenensis* revealed by its femora. C. R. Palevol 1, 1-13.

Pina, M., Alba, D.M., Moyà-Solà, S., Almécija, S., 2019. Femoral neck cortical bone distribution of dryopithecin apes and the evolution of hominid locomotion. J. Hum. Evol. 136, 102651.

Pirogov, N.I., 1853. An Illustrated Topographic Anatomy of Saw Cuts Made in Three Dimensions Across the Frozen Human Body. Vol. IV: Extrimitates. Yakob Trey, Petropoli.

Polk, J.D., Blumenfeld, J., Ahlumwalia, D., 2008. Knee posture predicted subchondral apparent density in the distal femur: An experimental validation. Anat. Rec. 291, 293-302.

Pontzer, H., Lieberman, D.E., Momin, E., Devlin, M.J., Polk, J.D., Hallgrímsson, B., Cooper, D.M.L., 2006. Trabecular bone in the bird knee responds with high sensitivity to changes in load orientation. J. Exp. Biol. 209, 57-65.

R Core Team, 2018. R: A language and environment for statistical computing. R Foundation for Statistical Computing, Vienna, Austria. http://www.R-project.org/.

Rafferty, K.L., 1998. Structural design of the femoral neck in primates. J. Hum. Evol. 34, 361-383.

Raichlen, D.A., Gordon, A.D., Foster, A.D., Webber, J.T., Sukhdeo, S.M., Scott, R.S., Gosman, J.H., Ryan, T.M., 2015. An ontogenetic framework linking locomotion and trabecular bone architecture with applications for reconstructing hominin life history. J. Hum. Evol. 81, 1-12.

Reed, K.E., Kitching, J., Grine, F.E., Jungers, W.L., Sokoloff, L., 1993. Proximal femur of *Australopithecus africanus* from Member 4, Makapansgat, South Africa. Am. J. Phys. Anthropol. 92, 1-15.

Reissis, D., Abel, R.L., 2012. Development of fetal trabecular micro-architecture in the humerus and femur. J. Anat. 220, 496-503.

Robinson, J.T., 1972. Early Hominid Posture and Locomotion. University of Chicago Press, Chicago.

Rose, M.D., 1977. Positional behaviour of olive baboons (*Papio anubis*) and its relationship to maintenance and social activities. Primates 18, 59-116.

Ruff, C.B., Burgess, M.L., Ketcham, R.A., Kappelman, J., 2016. Limb bone structural proportions and locomotor behavior in A.L. 288-1 ("Lucy"). PLoS One 11, e0166095.

Ruff, C.B., Higgins, R., 2013. Femoral neck structure and function in early hominins. Am. J. Phys. Anthropol. 150, 512-525.

Ryan, T.M., Carlson, K.J., Gordon, A.D., Jablonski, N. Shaw, C.N., Stock, J.T., 2018. Humanlike hip joint loading in *Australopithecus africanus* and *Paranthropus robustus*. J. Hum. Evol. 121, 12-24.

Ryan, T.M., Ketcham, R., 2002a. The three-dimensional structure of trabecular bone in the femoral head of strepsirrhine primates. J. Hum. Evol. 43, 1-26.

Ryan, T.M., Ketcham, R., 2002b. Femoral head trabecular bone structure in two omomyid primates. J. Hum. Evol. 43, 241-263.

Ryan, T.M., Ketcham, R., 2005. Angular orientation of trabecular bone in the femoral head and its relationship to hip joint loads in leaping primates. J. Morphol. 265, 249-263.

Ryan, T.M., Krovitz, G.E., 2006. Trabecular bone ontogeny in the human proximal femur. J. Hum. Evol. 51, 591-602.

Ryan, T.M., Shaw, C.N., 2012. Unique suites of trabecular bone features characterize locomotor behavior in human and non-human anthropoid primates. PLoS One 7, 1-11.

Ryan, T.M., Shaw, C.N., 2015. Gracility of the modern *Homo sapiens* skeleton is the result of decreased biomechanical loading. Proc. Natl. Acad. Sci. USA 112, 372-377.

Ryan, T.M., Walker, A., 2010. Trabecular bone structure in the humeral and femoral heads of anthropoid primates. The Anat. Rec. 293, 719-729.

Saparin, P., Scherf, H., Hublin, J.-J., Fratzl, P., Weinkamer, R., 2011. Structural adaptation of trabecular bone revealed by position resolved analysis of proximal femora of different primates. Anat. Rec. 294, 55-67.

Sas, A., Pellikaan, P., Kolk, S., Marty, P., Scheerlinck, T., Harry van Lenthe, G., 2019. Effect of anatomical variability on stress-shielding induced by short calcar-guided stems: Automated finite element analysis of 90 femora. J. Orthop. Res. 37, 681-688.

Senut, B., Pickford, M., Gommery, D., Mein, P., Cheboi, K., Coppens, Y., 2001. First hominid from the Miocene (Lukeino Formation, Kenya). C. R. Acad. Sci. Paris 332, 137-144.

Shaw, C., Ryan, T., 2012. Does skeletal anatomy reflect adaptation to locomotor patterns? Cortical and trabecular architecture in human and nonhuman anthropoids. Am. J. Phys. Anthropol. 147, 187-200.

Skerry, T.M., Lanyon, L.E., 1995. Interruption of disuse by short duration walking exercise does not prevent bone loss in the sheep calcaneus. Bone 16, 269-274.

Stern, J.T., Susman, R.L., 1991. "Total morphological pattern" versus the "magic trait": Conflicting approaches to the study of early hominid bipedalism. In: Coppens, Y., Senut, B. (Eds.), Origine(s) de la Bipédie chez les Hominidés. CNRS, Paris, pp. 99-111.

Stiles, R.G., Laverina, C.J., Resnick, D., Convery, F.R., 1990. The calcar femorale. An anatomic, radiologic, and surgical correlative study. Invest. Radiol. 25, 1311-1315.

Susman, R.L., de Ruiter, D., Brain, C.K., 2001. Recently identified postcranial remains of *Paranthropus* and early *Homo* from Swartkrans Cave, South Africa. J. Hum. Evol. 41, 607-629.

Tatu, L., Parratte, B., Vuillier, F., Diop, M., Monnier, G., 2002. Descriptive anatomy of the femoral portion of the iliopsoas muscle. Anatomical basis of anterior snapping of the hip. Surg. Radiol. Anat. 23, 371-374.

Tetsunaga, T., Fujiwara, K., Endo, H., Tetsunaga, T., Shiota, N., Sato, T., Ozaki, T., 2017. Calcar femorale in patients with osteoarthritis of the hip secondary to developmental dysplasia. Clin. Orthop. Surg. 9, 413-419.

Thakkar, C.J., Thakkar, S., Kathalgere, R.T., Kumar, M.N., 2015. Calcar femorale grafting in the hemiarthroplasty of the hip for unstable inter trochanteric fractures. Indian J. Orthop. 49, 602-609.

Thompson, R., 1907. The relationship between the internal structure of the upper part of the femur and fractures through the base of the neck of the femur. J. Anat. Physiol. 42, 60-68.

Thorpe, S.K.S., Crompton, R.H., 2006. Orangutan positional behavior and the nature of arboreal locomotion in Hominoidea. Am. J. Phys. Anthropol. 131, 384-401.

Thorpe, S.K.S., Holder, R.L., Crompton, R.H., 2007. Origin of human bipedalism as an adaptation for locomotion on flexible branches. Science 316, 1328-1331.

Tsegai, Z.J., Skinner, M.M., Pahr, D.H., Hublin, J.-J., Kivell, T.L., 2018a. Systemic patterns of trabecular bone across the human and chimpanzee skeleton. J. Anat. 232, 641656.

Tsegai, Z.J., Skinner, M.M., Pahr, D.H., Hublin, J.-J., Kivell, T.L., 2018b. Ontogeny and variability of trabecular bone in the chimpanzee humerus, femur and tibia. Am. J. Phys. Anthropol. 167, 713-736.

Vera, M.C., Ferretti, J.L., Abdala, V., Cointry, G.R., 2020. Biomechanical properties of anuran long bones: correlations with locomotor modes and habitat use. J. Anat. 236, 1112-1125.

Volpato, V., Viola, T.B., Nakatsukasa, M., Bondioli, L., Macchiarelli, R., 2008. Textural characteristics of the iliac-femoral trabecular pattern in a bipedally-trained Japanese macaque. Primates 49, 16-25.

Wallace, I.J., Burgess, M.L., Patel, B.A., 2020. Phalangeal curvature in a chimpanzee raised like a human: Implications for inferring arboreality in fossil hominins. Proc. Natl. Acad. Sci. USA 117, 11223-11225.

Wallace, I.J., Kwaczala, A.T., Judex, S., Demes, B., Carlson, K.J., 2013. Physical activity engendering loads from diverse directions augments the growing skeleton. J. Muscul. Neuron. Int. 13, 283-288.

Wallace, I.J., Tommasini, S.M., Judex, S., Garland, T., Demes, B., 2012. Genetic variations and physical activity as determinants of limb bone morphology: An experimental approach using a mouse model. Am. J. Phys. Anthropol. 148, 24-35.

Wang, J.P., Yang, T.F., Zhong, F.L., 2005. Finite element analysis of the biomechanics of human femur (Chin). Zhonghua Chuang Shang Gu Ke Za Zhi 7, 931-934.

Ward, C.V., 2013. Postural and locomotor adaptations of *Australopithecus* species. In: Reed, K.E., Fleagle, J.G., Leakey, R.E. (Eds.), The Paleobiology of *Australopithecus*. Springer, Dordrecht, pp. 235-245.

Ward, C.V., Feibel, C.S., Hammond, A.S., Leakey, L.N., Moffett, E.A., Plavcan, J.M., Skinner, M.M, Spoor, F., Leakey, M.G., 2015. Associated ilium and femur from Koobi Fora, Kenya, and postcranial diversity in early *Homo*. J. Hum. Evol. 81, 48-67.

Ward, C.V., Hammond, A.S., Plavcan, J.M., Begun, D.R., 2019. A late Miocene hominid partial pelvis from Hungary. J. Hum. Evol. 136, 102645.

White, T.D., 1984. Pliocene hominids from Middle Awash, Ethiopia. Cour. Forsch-Inst. Sencken. 69, 57-68.

Wickham, H., 2009. ggplot2: Elegant Graphics for Data Analysis. Springer-Verlag, New York.

Williams, S.A., Prang, T.C., Meyer, M.R., Russo, G.A., Shapiro, L.J., 2020. Reevaluating bipedalism in *Danuvius*. Nature 586, E1-E3.

Wood, B., Constantino, P., 2007. *Paranthropus boisei*: Fifty years of evidence and analysis. Am. J. Phys. Anthropol. 134, 106-132.

Wood, B., Leakey, M., 2011. The Omo-Turkana Basin fossil hominins and their contribution to our understanding of human evolution in Africa. Evol. Anthropol. 20, 264-292.

Wroblewski, B., Siney, P.D., Fleming, P.A., Bobak, P., 2000. The calcar femorale in cemented stem fixation in total hip arthroplasty. J. Bone Joint Surg. 82, 842-845.

Zha, G.C., Liu, J., Wang, Y., Feng, S., Chen, X.Y., Guo, K.J., Sun, J.Y., 2019. Cementless distal fixation modular stem without reconstruction of femoral calcar for unstable intertrochanteric fracture in patients aged 75 years or more. Ortho. Traum. Surg. Res. 105, 35-39.

Zhang, Q., Chen, W., Liu, H.J., Li, Z.Y., Song, Z.H., Pan, J.S., Zhang, Y.Z., 2009. The role of the calcar femorale in stress distribution in the proximal femur. Ortho. Surg. 1, 311-316.

Zipfel, B., Richmond, B.G., Ward, C.V., 2020. Hominin Postcranial Remains from Sterkfontein, South Africa, 1936-1995. Oxford University Press, Oxford.

Figures captions

Figure 1. Micro-CT-scanned transverse (upper; blue outline) and parasagittal (lower; yellow outline) virtual sections, extracted respectively at the upper margin and at the center of the lesser trochanter showing the calcar femorale a) absence and b) presence (b; arrows) in two extant human individuals.

Figure 2. Micro-CT-based measurements (black lines) of the calcar femorale (CF) in a virtually-rendered human right proximal femur shown in semitransparency in posterior view (a, b, d) and on a virtual transverse section across the lesser trochanter of the same specimen at the level of the maximum width of the calcar femorale (CF) root (c). In all cases, medial is to the left. a) PT MaxLength, measured as maximum distance between the periosteal contour and the CF most internal point; in the colored map, the CF increasing distance from the periosteal contour is rendered by a chromatic scale ranging from turquoise to red. b) CF MaxLength, measured as maximum projective distance between the base of the CF root on the endosteal contour and its most internal point. c) CF MaxHeight, measured as maximum projected distance between the uppermost (upper view) and the lowest (lower view) virtually extracted slices bearing evidence of a CF-related spur of thickened bone. d) CF root max width. Scale bar = 10 mm.

Figure 3. Micro-CT-based transverse (upper left) and parasagittal (right) virtual sections respectively extracted at the upper margin and at the center of the lesser trochanter showing the CF presence (indicated with an arrow)/absence and extension in selected proximal femora representing five extant human, *Pan*, *Gorilla*, *Pongo*, and *Papio* individuals (a–e). Independent of

their original side, all specimens are imaged as right femora. See SOM Figure S3 for the additional extant specimens. Scale bar = 10 mm.

Figure 4. Micro-CT-based 3D rendering of the calcar femorale (CF; in red) in an extant human, a *Pan*, a *Gorilla*, and a *Pongo* right femur, virtually shown in semitransparency in a) anterior, b) lateral, c) posterior, and d) medialview. Scale bar = 10 mm.

Figure 5. Boxplots of the absolute (upper row) and standardized (lower row) values of the variables PT MaxLength (measured as maximum distance between the periosteal contour and the CF most internal point, CF MaxLength (measured as maximum projective distance between the base of the CF root on the endosteal contour and its most internal point), and CF MaxHeight (measured as maximum projected distance between the uppermost and lowest virtually extracted slices bearing evidence of a CF-related spur of thickened bone) measured in the extant human, *Pan*, and *Gorilla* samples and in one *Pongo* individual, as well as the absolute individual values (upper row) of CF MaxLength and CF MaxHeight measured in the fossil hominid specimens representing *Rudapithecus* (RUD 234), *A. africanus* (StW 99 and 367), and likely *P. boisei* (KNM-ER 738 and 1465). The asterisks indicate statistically significant inter-taxa comparisons (pairwise Wilcoxon rank sum test); the black-closed circle (CF MaxHeight in the lower row) indicates an outlier. No estimate is available in StW 367 for CF MaxHeight. The center horizontal line represents the median, the interquartile range is represented by the box, maximum and minimum values of the data excluding potential outliers are represented by vertical lines, and outliers are represented by black circles bellow and above 1.5 times the interquartile range).

Figure 6. Micro-CT-based transverse (upper, blue outline) and parasagittal (lower, yellow outline) virtual sections, extracted respectively at the upper margin and at the center of the lesser trochanter showing the calcar femorale (CF) presence/absence in the fossil hominid specimens representing, from left to right and top-down, *Rudapithecus* (RUD 234), *A. africanus* (StW 99 and, 367), *P. robustus* (SK 97), and likely *P. boisei* (KNM-ER 738 and 1465). The white arrows indicate the CF. We observed no trace of a CF in SK 97, although possible strengthening of the trabeculae projecting towards the greater trochanter could not be confidently ascertained because of the incomplete preservation in this specimen. Independent of their original side, all specimens are imaged as right femora (for their original side, see SOM Table S2). Scale bar = 10 mm.

Figure 7. Micro-CT-based 3D rendering of the calcar femorale (CF; in red) in RUD 234 (*Rudapithecus*) left femur (here imaged as right) and KNM-ER 738 (likely *P. boisei*) right femur, virtually shown in semitransparency in a) anterior, b) lateral, c) posterior, and d) medial view. Compare with the μCT-based 3D rendering of the CF (in red) in an extant human, a *Pan*, a *Gorilla*, and a *Pongo* right femur, virtually shown in semitransparency in anterior view, showing a more important vertical height of the CF in humans compared with great apes, with a CF extended into the lower part of the lesser trochanter in humans and typically confined to the proximal half of the lesser trochanter compartment in great apes. Scale bar = 10 mm.

Table 1

Absolute and standardized values (in mm) of the calcar femorale (CF) maximum length from the periosteal contour (PT MaxLength; see Fig. 2a), CF maximum length from the endosteal contour (CF MaxLength; see Fig. 2b) and CF maximum height (CF MaxHeight; see Fig. 2c) measured in the extant human, *Pan*, and *Gorilla* samples and in one *Pongo* individual. For each taxon, sample size (*n*), mean (or individual value), standard deviation (in parentheses), and range of variation are provided.

Taxon	PT MaxLength	CF MaxLength	CF MaxHeight
Absolute values			
Extant humans	12.2 (2.2)	9.9 (1.8)	35.9 (7.9)
(*n* = 9)	8.4–13.9	6.3–11.9	22.3–46.2
Pan	7.8 (1.5)	6.2 (1.6)	13.3 (4.4)
(*n* = 6)	5.9–10.3	3.7–8.1	7.1–19.1
Gorilla	9.7 (4.2)	7.8 (3.5)	22.0 (6.5)
(*n* = 6)	3.7–15.3	3.5–12.7	15.2–31.6
Pongo (*n* = 1)	11.6	8.0	18.0
Standardized values[a]			
Extant humans	0.22 (0.05)	0.18 (0.05)	0.64 (0.15)
(*n* = 9)	0.16–0.31	0.12–0.27	0.47–0.93
Pan	0.18 (0.05)	0.15(0.04)	0.32 (0.13)
(*n* = 6)	0.12–0.26	0.08–0.19	0.15–0.48
Gorilla	0.09 (0.03)	0.07 (0.03)	0.22 (0.12)
(*n* = 6)	0.05–0.12	0.03–0.12	0.10–0.45
Pongo (*n* = 1)	0.14	0.10	0.22

[a]Absolute values were standardized by body mass estimated for each individual from their femoral head diameter by using the equations provided by Ruff et al. (2018) for humans and Burgess et al. (2018) for extant apes.

Table 2

Absolute values (in mm) of calcar femorale (CF) maximum length from the endosteal contour (CF MaxLength; see Fig. 2b) and CF maximum height (CF MaxHeight; see Fig. 2c) measured in the fossil hominid sample.

Taxon/ specimen	CF MaxLength	CF MaxHeight
Rudapithecus hungaricus RUD 234	8.5	14.9
Australopithecus africanus StW 99	5.6	28.7
StW 367	4.8	—
Paranthropus boisei? KNM-ER 738	6.2	18.5
KNM-ER 1465	7.5	26.4

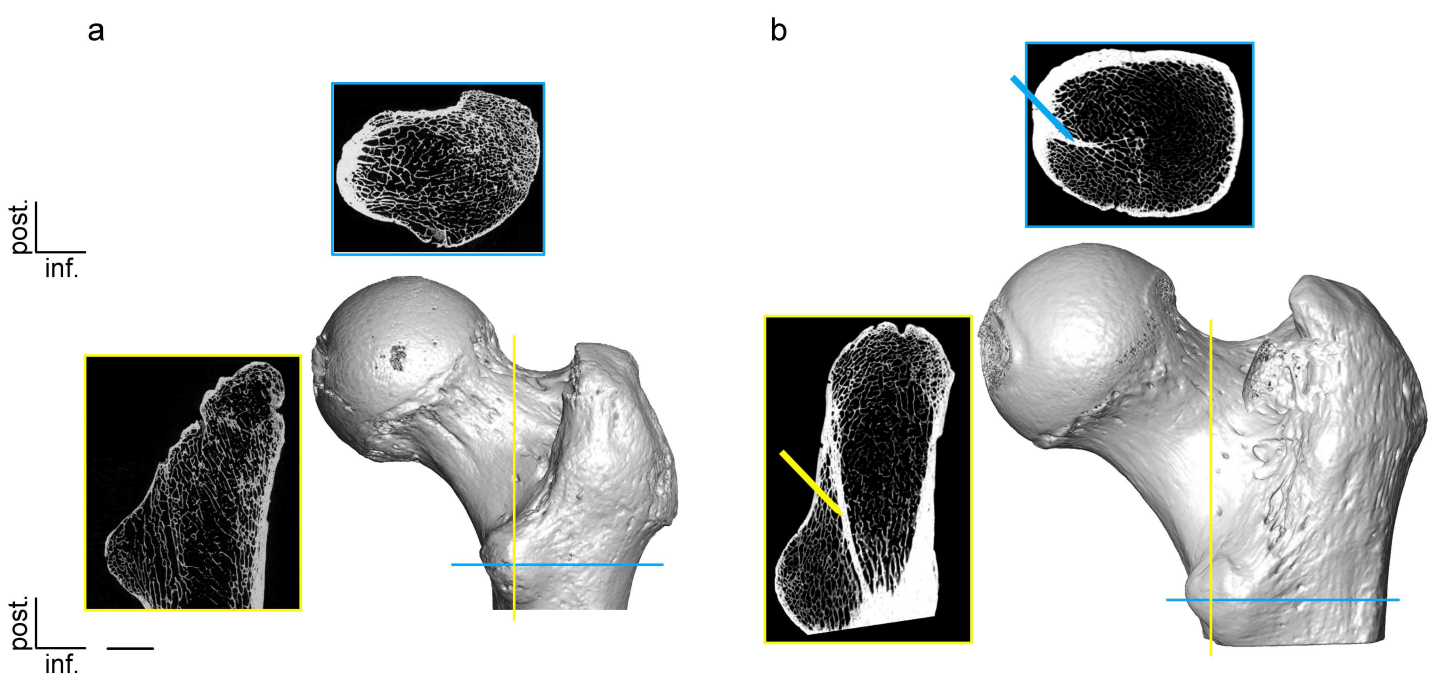
a
post.
inf.
post.
inf.
b

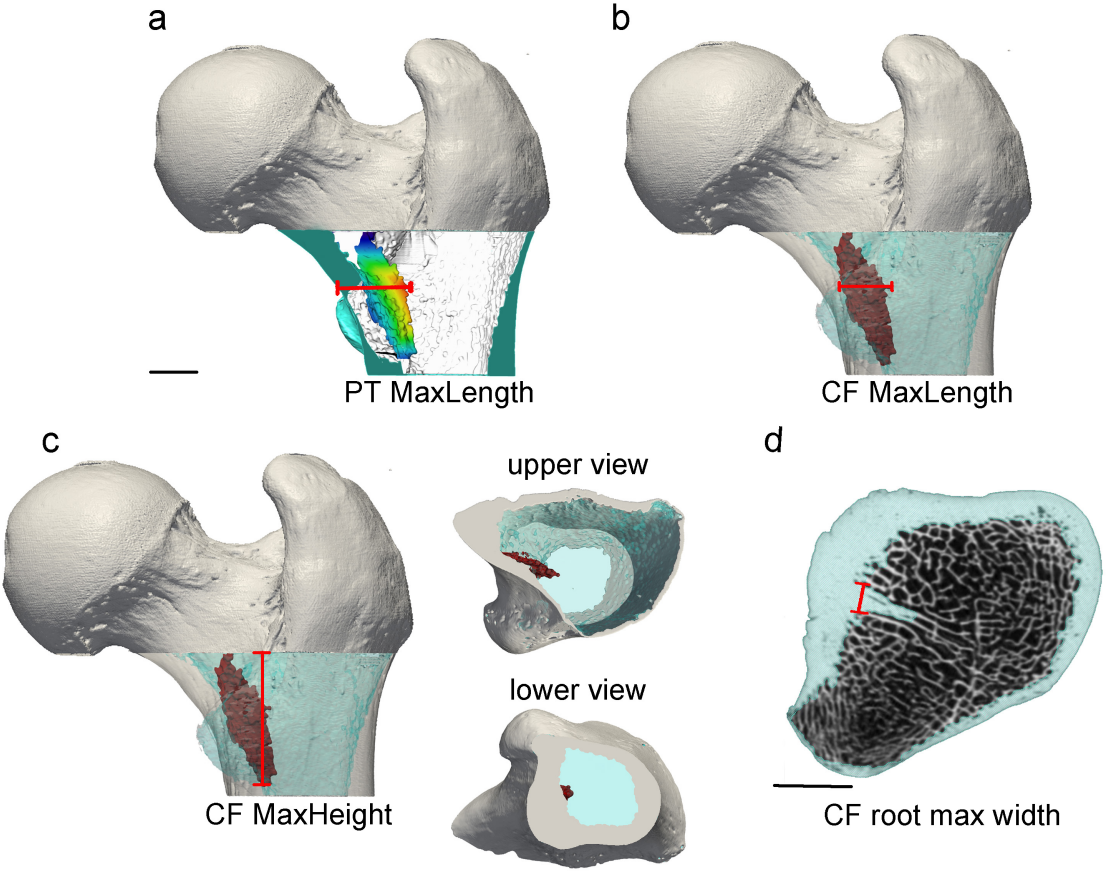
a
PT MaxLength
b
CF MaxLength
c
CF MaxHeight
upper view
lower view
d
CF root max width

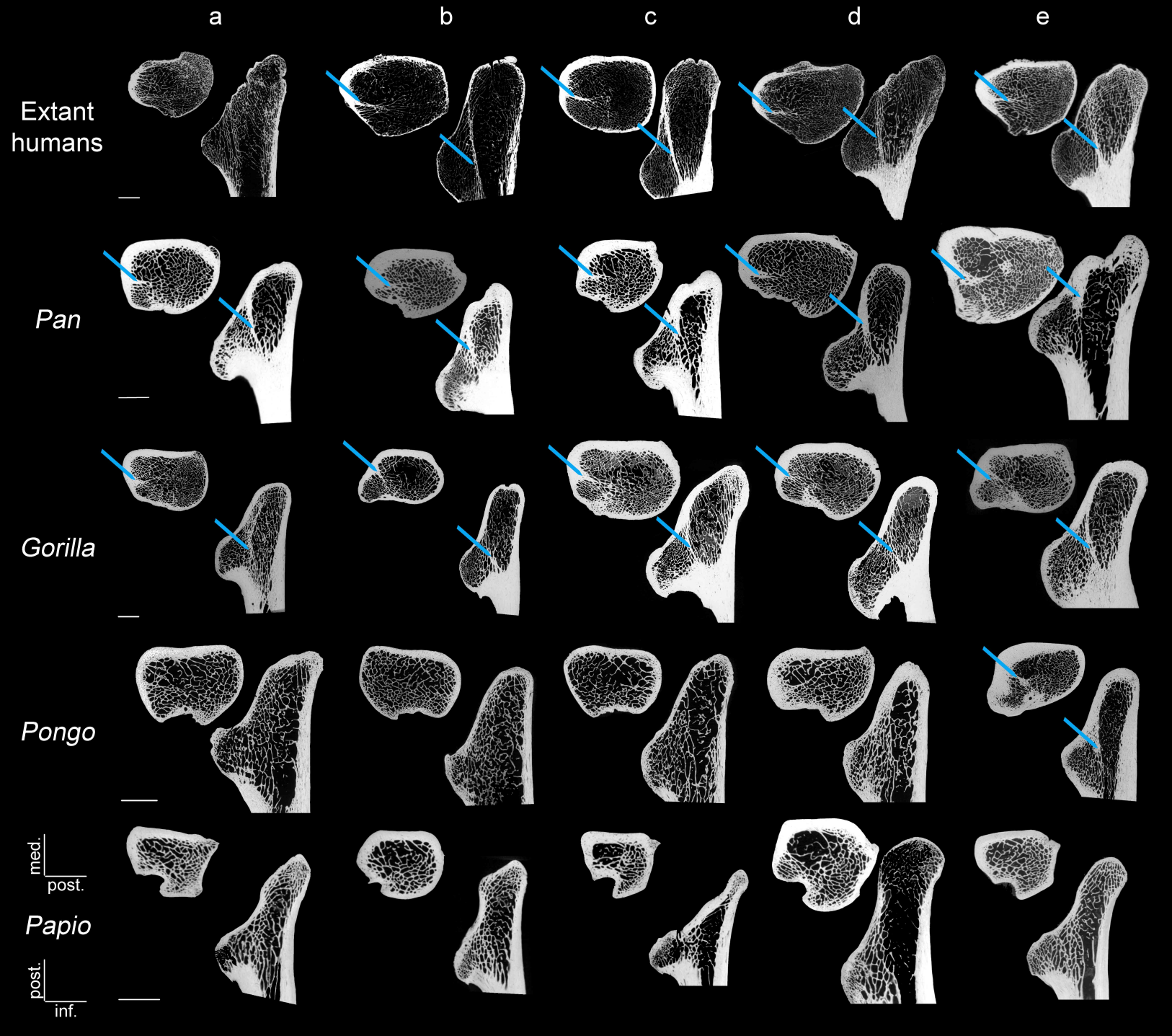
a
b
c
d
e
Extant humans
Pan
Gorilla
Pongo
Papio
med.
post.
post.
inf.

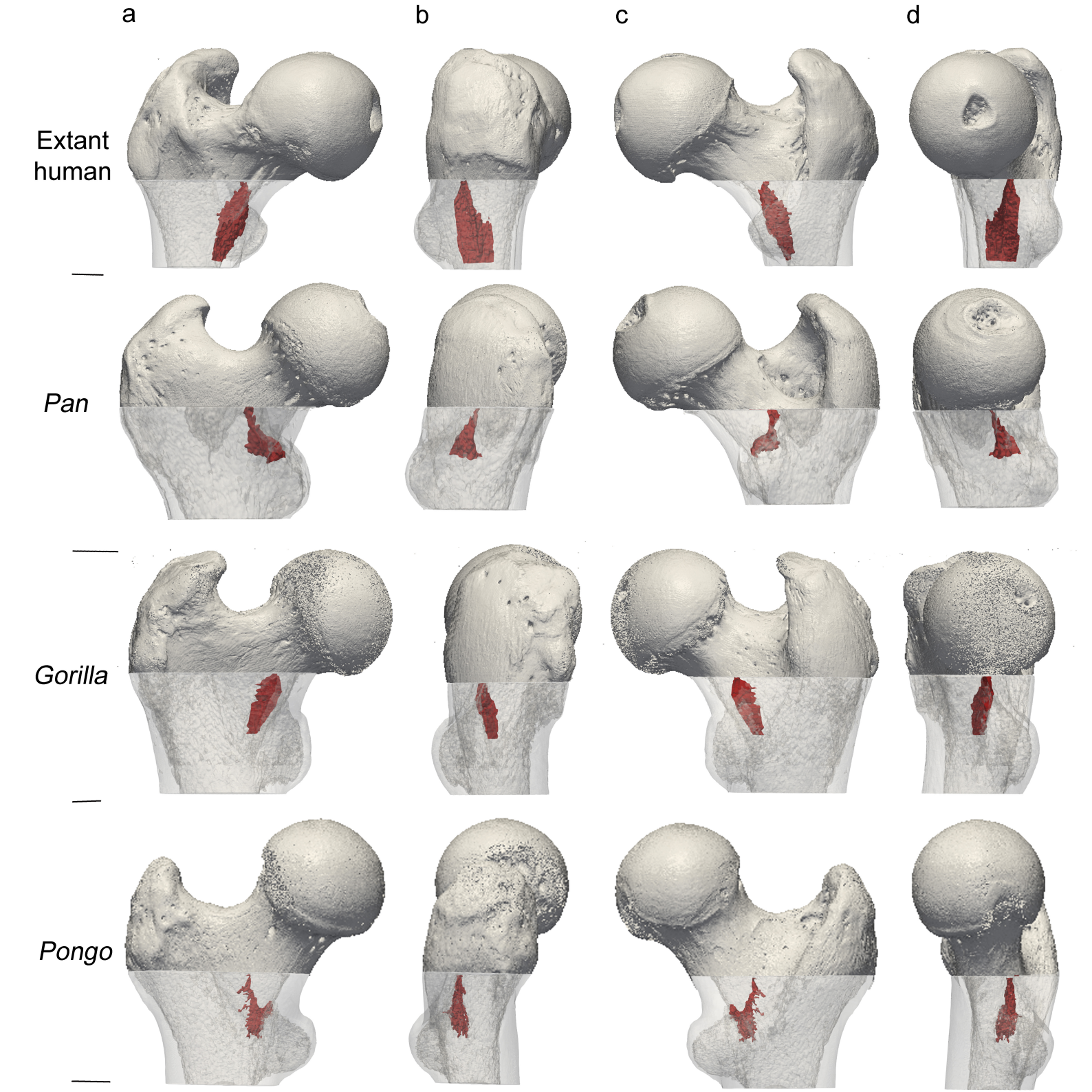
a
b
c
d
Extant human
Pan
Gorilla
Pongo

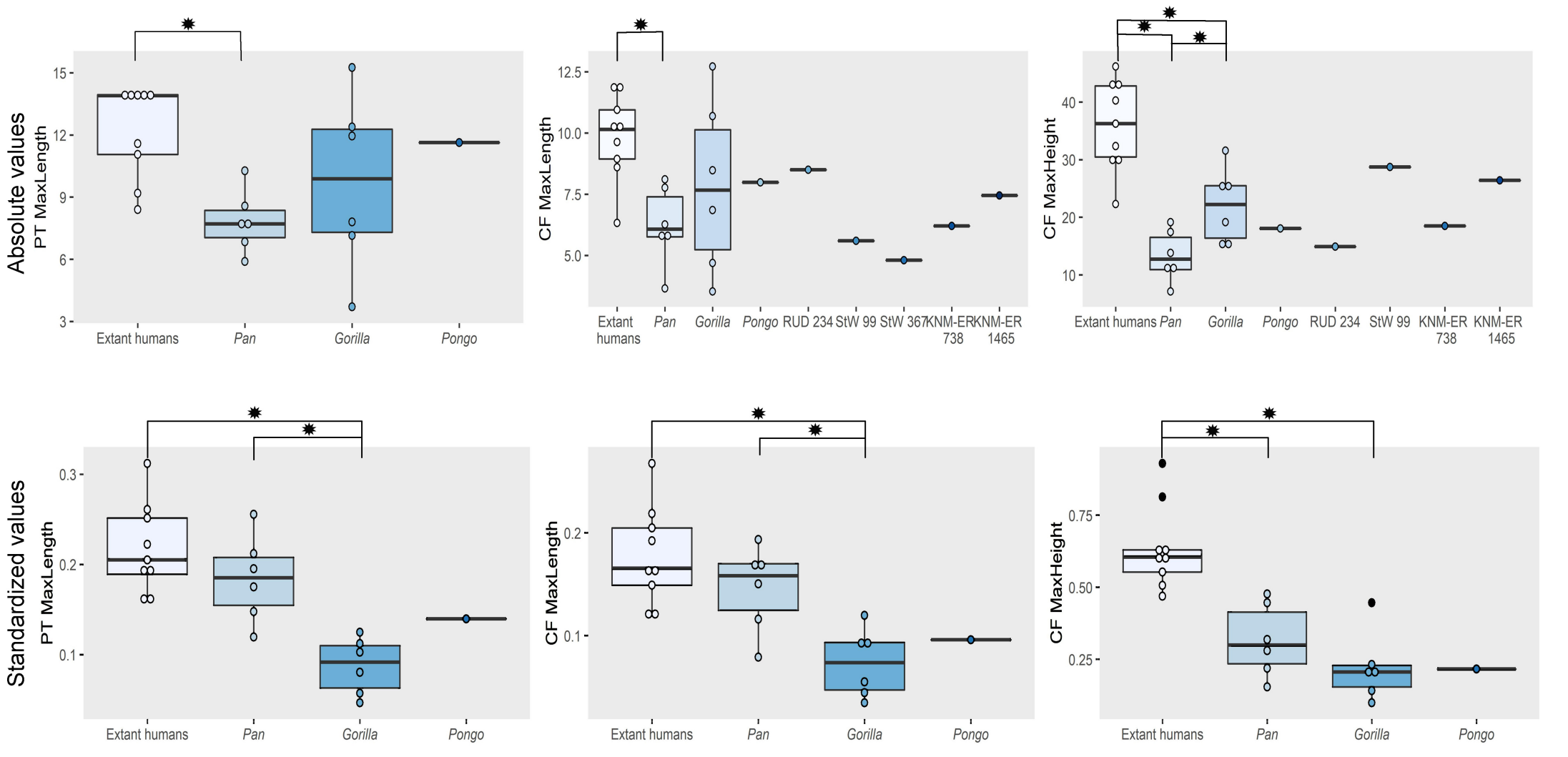
Absolute values
Standardized values
PT MaxLength
CF MaxLength
CF MaxHeight
Extant humans
Pan
Gorilla
Pongo
RUD 234
StW 99
StW 367
KNM-ER 738
KNM-ER 1465

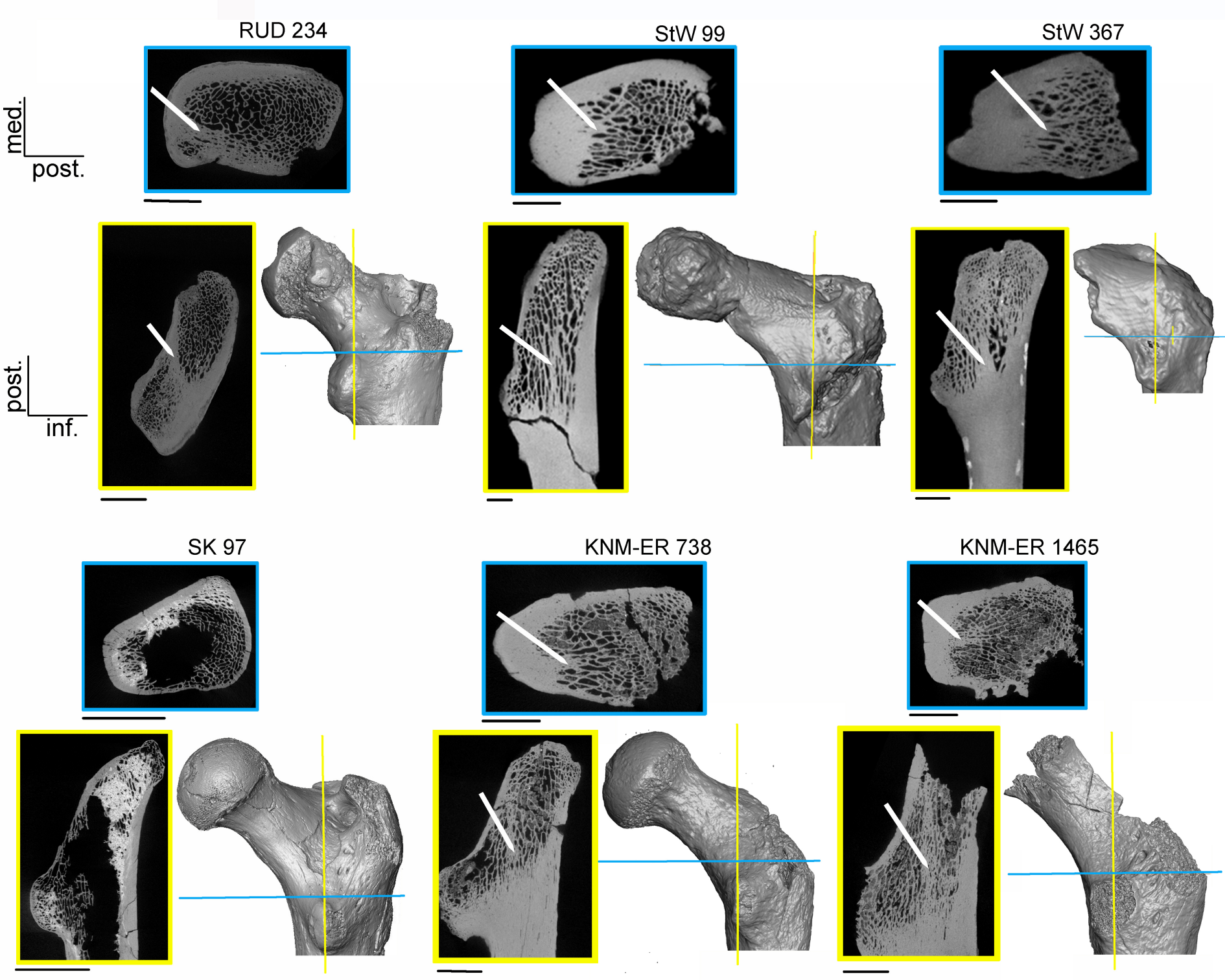
RUD 234
StW 99
StW 367
med.
post.
post.
inf.
SK 97
KNM-ER 738
KNM-ER 1465

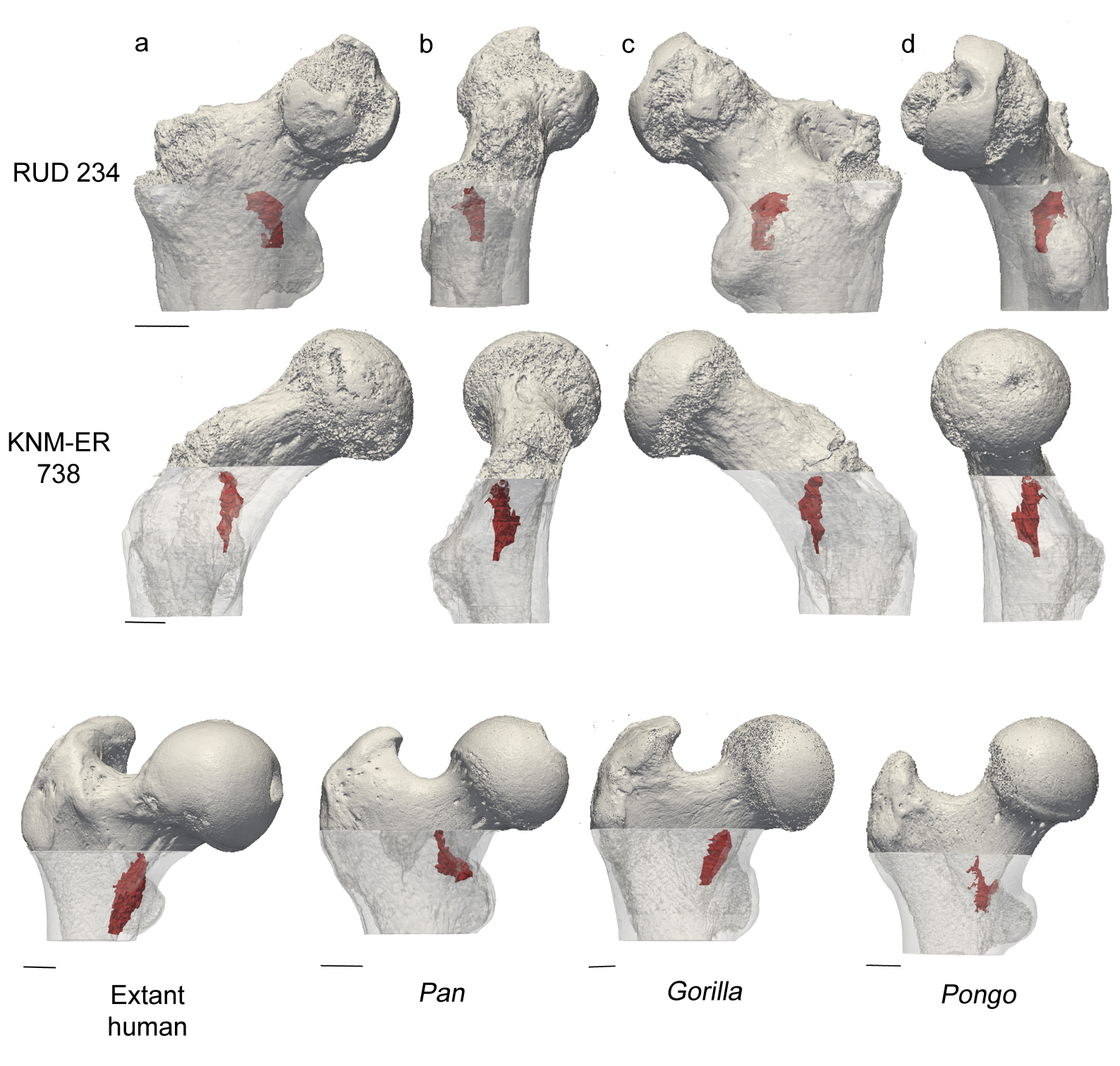
a
b
c
d
RUD 234
KNM-ER 738
Extant human
Pan
Gorilla
Pongo

Supplementary Online Material (SOM):

Calcar femorale variation in extant and fossil hominids: Implications for identifying bipedal locomotion in fossil hominins

Marine Cazenave [a,b,*], Tracy L. Kivell [a,c,d], Marta Pina [e,f], David R. Begun [g], Matthew M. Skinner [a,c,d]

[a] *Skeletal Biology Research Centre, School of Anthropology and Conservation, University of Kent, Canterbury, UK*

[b] *Department of Anatomy, Faculty of Health Sciences, University of Pretoria, South Africa*

[c] *Department of Human Evolution, Max Planck Institute for Evolutionary Anthropology, Leipzig, Germany*

[d] *Centre for the Exploration of the Deep Human Journey, University of the Witwatersrand, Johannesburg, South Africa*

[e] *Interdisciplinary Centre for Ancient Life, School of Natural Sciences, University of Manchester, Manchester, UK*

[f] *Institut Català de Paleontologia Miquel Crusafont, Universitat Autònoma de Barcelona, Cerdanyola del Vallès, Spain*

[g] *Department of Anthropology, University of Toronto, Toronto, Ontario, Canada*

Corresponding author.

Email address: marine.cazenave4@gmail.com (M. Cazenave)

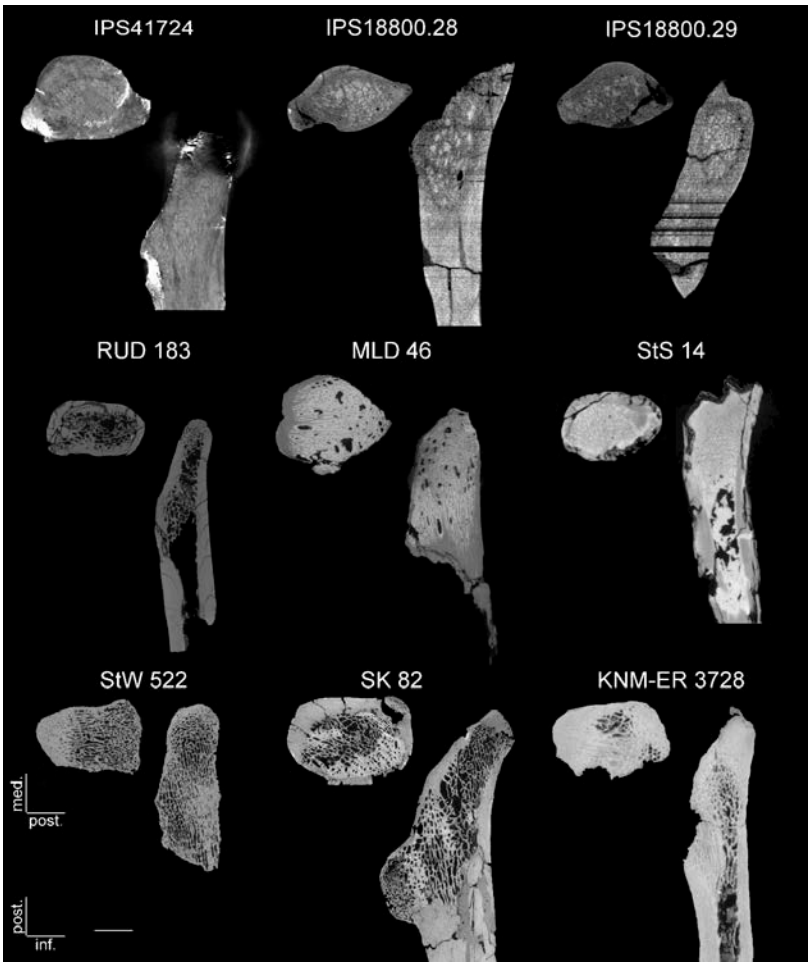

SOM Figure S1. Micro-CT-based transverse (upper left) and parasagittal (right) virtual sections extracted at the upper margin and at the center of the lesser trochanter, respectively, showing the preservation conditions of the fossil hominid and hominin specimens unsuitable for the assessment of the calcar femorale presence/absence because the area of interest is not well-preserved. All specimens are imaged as right femora. Scale bar = 10 mm.

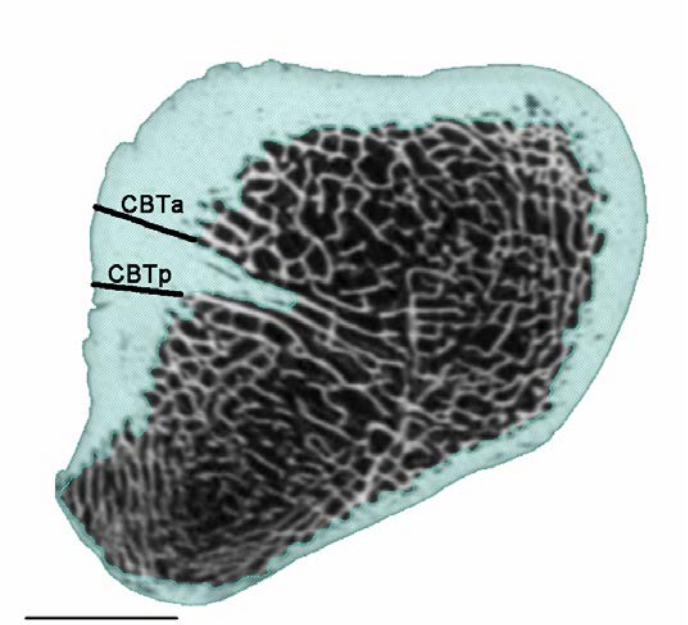

SOM Figure S2. Micro-CT-based cortical bone thickness (CBT) measured at the anterior (CBTa) and posterior (CBTp) limits of the calcar femorale (CF) root on a transverse virtual section across the lesser trochanter of a human right femur (specimen number X818) at the level of the maximum width of the CF root (see Fig. 2c in the main text). Scale bar = 10 mm.

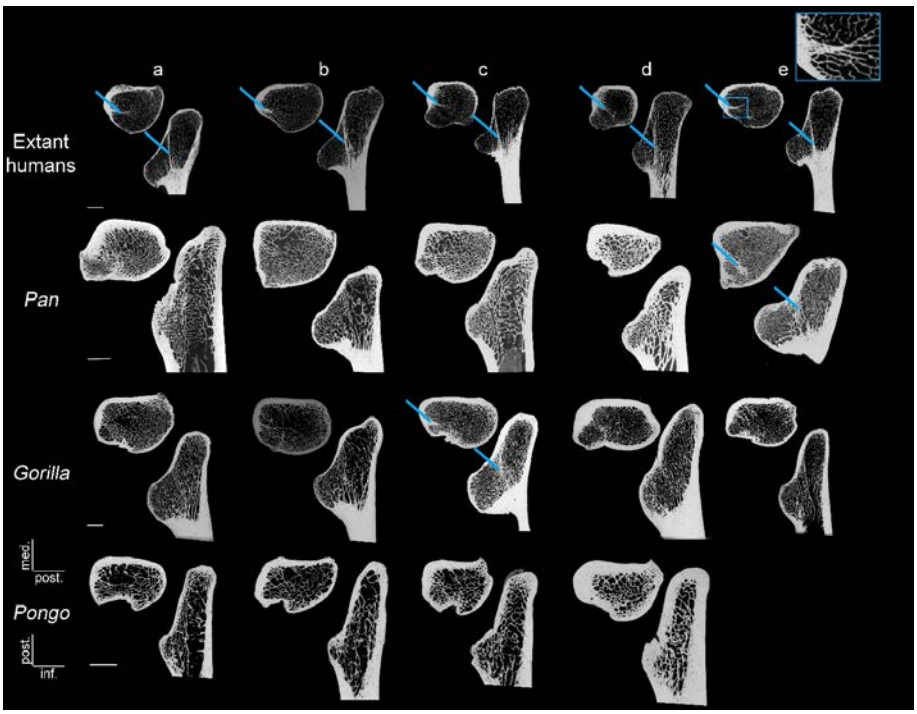

SOM Figure S3. Micro-CT-based transverse (upper left) and parasagittal (right) virtual sections, extracted at the upper margin and at the center of the lesser trochanter, respectively, showing the calcar femorale presence/absence and extension in the proximal femora representing the extant humans, *Pan, Gorilla,* and *Pongo* that are not shown in Figure 3 in the main text. All specimens are imaged as right femora regardless of their original side. Scale bar = 10 mm.

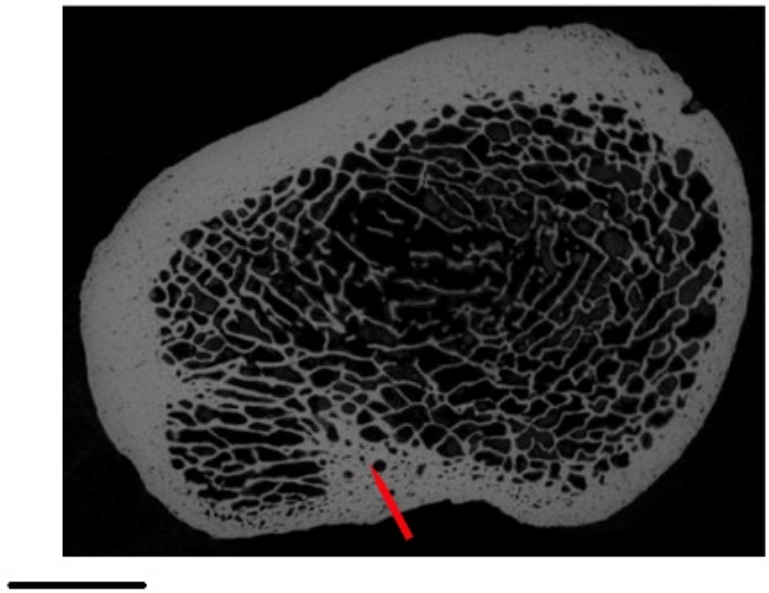

SOM Figure S4. Micro-CT-based transverse virtual section across the lesser trochanter of a *Gorilla* right femur (specimen number MER_264) showing a bone reinforcement at the lateral margin of the lesser trochanter (red arrow) radiating medially towards the calcar femorale (left). Scale bar = 10 mm.

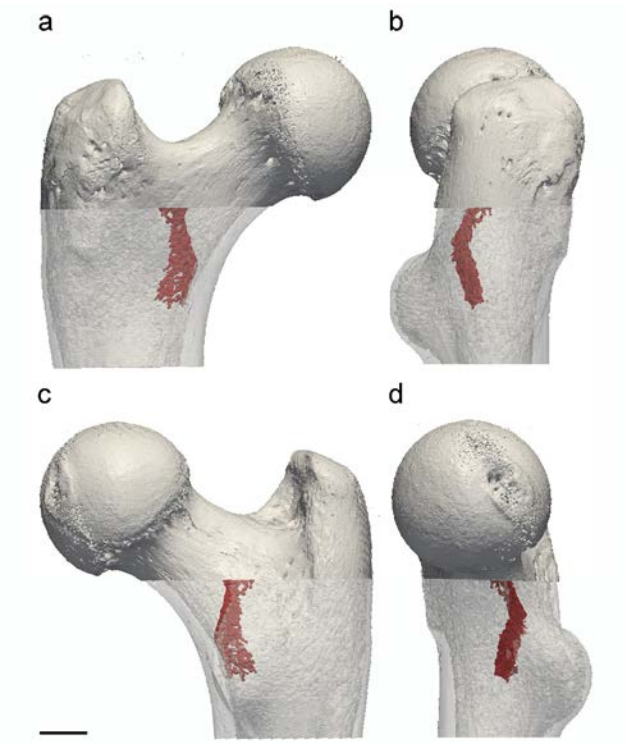

SOM Figure S5. Micro-CT-based 3D rendering of an especially proximodistally developed calcar femorale (in red) in a female *Gorilla* right femur (specimen number MER_856) virtually shown in semitransparency in a) anterior, b) lateral, c) posterior, and d) medial views. Scale bar = 10 mm.

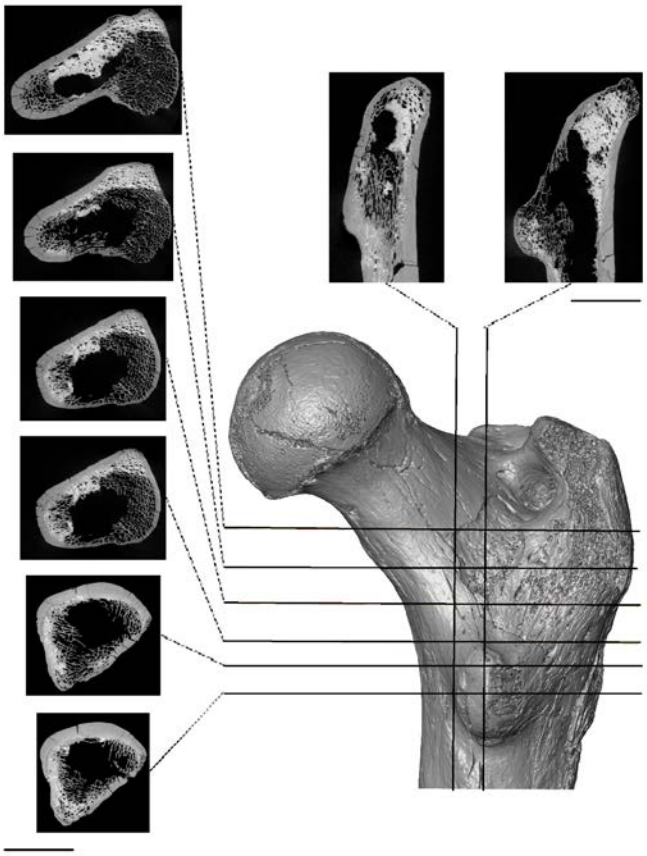

SOM Figure S6. Micro-CT-based 3D rendering in posterior view (lower right) of the SK 97 *Paranthropus robustus* right proximal femur from Swartkrans, South Africa, with indication of the position (black lines) of two parasagittal (upper right) and six transverse (left) virtual sections extracted across the region of interest, showing no trace of a calcar femorale (compare with Fig. 6 in the main text). Scale bar = 10 mm.

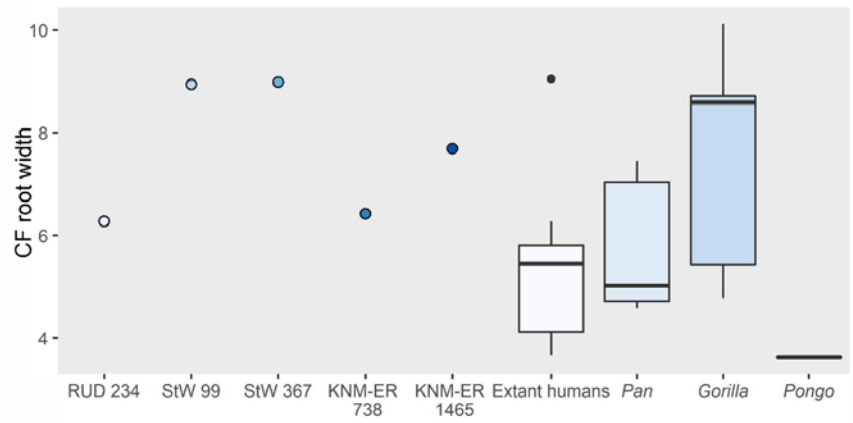

SOM Figure S7. Boxplot of the absolute values (in mm) of maximum width of the calcar femorale (CF) root (CF root width) measured in the fossil hominid specimens representing *Rudapithecus* (RUD 234), *A. africanus* (StW 99 and 367), and likely *P. boisei* (KNM-ER 738 and 1465) compared to the values measured in the extant human (n = 8), *Pan* (n = 5), and *Gorilla* (n = 5) samples and in one *Pongo* individual. Center horizontal line marks the median, interquartile range is represented by the box, maximum and minimum values are represented by vertical lines.

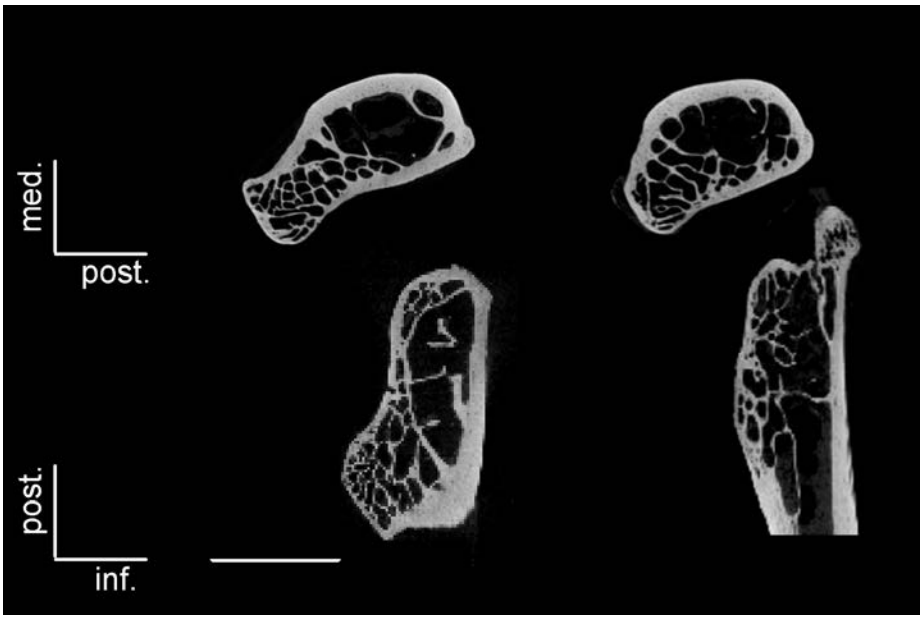

SOM Figure S8. Micro-CT-based transverse (upper left) and parasagittal (right) virtual sections, extracted at the upper margin and at the center of the lesser trochanter, respectively, showing the absence of the calcar femorale in two right proximal femora representing *Hylobates lar*. Scale bar = 10 mm.

Comentado [A1]: Please remind readers here of the key point of this figure i.e., no indication of a CF

SOM Table S1

Origin, composition, and µCT scanning information for the extant hominid samples.

Specimen	Sex	Age (years)	Ancestry/provenance	Behavior/subsistence/ condition	Collection[b]	Scan location[c]	Voxel size (µm)
Extant humans[a] (*n* = 10)							
MMK X08	M	30–49	Khoesan	hunter gatherer	McGM	ESI	67
MMK 2X3	F	44–54	Khoesan	hunter gatherer	McGM	ESI	70
MMK 23X	F	30s	Khoesan	hunter gatherer	McGM	ESI	67
MMK X36	F	32–52	Khoesan	hunter gatherer	McGM	ESI	70
X926	M	41	European	likely sedentary	PBC	NECSA	69
5X55	M	51	European	likely sedentary	PBC	NECSA	67
56X6	M	51	European	likely sedentary	PBC	NECSA	67
576X	F	32	African	NA	PBC	NECSA	69
X818	F	50	European	likely sedentary	PBC	NECSA	50
5X78	F	32	African	NA	PBC	NECSA	69
Pan troglodytes (*n* = 10)							
Za 1355	M?	A	NA	wild?	ESI	ESI	42
A12761	F	A	Gabon	wild	MNHN	MNHN	80
ZM-AC_1950-194	M	A	Congo	wild	MNHN	MNHN	73
ZM-AC_1899-17	M	A	NA	NA	MNHN	MNHN	80
ZM-AC_1923-2497	F?	A	NA	NA	MNHN	MNHN	67
ZM-AC_1936-630	F	A	NA	NA	MNHN	MNHN	73
ZM-AC_1947-149	F	A	NA	NA	MNHN	MNHN	66
ZM-AC_1966-332	F	A	NA	NA	MNHN	MNHN	73
MPITC-11782	M	A	Ivory Coast	wild	MPIEVA	MPIEVA	30
MPITC-15012	M	A	Ivory Coast	wild	MPIEVA	MPIEVA	38
Gorilla gorilla (*n* = 10)							

CAMI_106	M	A	Cameroon	wild	PCM	CBC	75
MER_95	F	A	Cameroon	wild	PCM	CBC	54
MER_96	F	A	Cameroon	wild	PCM	CBC	48
MER_135	M	A	Cameroon	wild	PCM	CBC	60
MER_264	M	A	Cameroon	wild	PCM	CBC	58
MER_300	F	A	Cameroon	wild	PCM	CBC	60
MER_372	M	A	Cameroon	wild	PCM	CBC	63
MER_729	M	A	Cameroon	wild	PCM	CBC	62
MER_798	F	A	Cameroon	wild	PCM	CBC	48
MER_856	F	A	Cameroon	wild	PCM	CBC	45
Pongo sp. (*n* = 9)							
ZSM_1907_0331	NA	A	NA	NA	ZSM	MPIEVA	28
ZSM_1907_0483	F	A	Borneo	wild	ZSM	MPIEVA	28
ZSM_1907_0633b	F	A	Borneo	wild	ZSM	MPIEVA	28
ZSM_1907_0660	F	A	Borneo	wild	ZSM	MPIEVA	29
ZSM_1909_0801	M	A	Borneo	wild	ZSM	MPIEVA	29
ZSM_1955_0228	F	A	Zoo Hellabrunn, from Singapore	wild	ZSM	MPIEVA	28
ZSM_1966_0203	M	A	Zoo Hannover, Germany	captive	ZSM	MPIEVA	29
ZSM_1973_0270	Na	A	Sumatra	wild	ZSM	MPIEVA	28
ZSM_1982/0092	F	A	Zoo Hannover, Germany	captive	ZSM	MPIEVA	28
Papio ursinus (*n* = 5)							
03	NA	A	South Africa	wild	PBC	NECSA	67
18	NA	A	South Africa	wild	PBC	NECSA	61
19	NA	A	South Africa	wild	PBC	NECSA	64
22	NA	A	South Africa	wild	PBC	NECSA	61
UCT-1703	NA	A	Cape Town, South Africa	wild	UCT	NECSA	45

Abbreviations: A = adult; F = female; M = male; NA = information not available.

[a] Following South African stipulations, one digit within each individual label has been replaced by an 'X', to keep individual identity confidential.

[b] ESI = Evolutionary Studies Institute of the University of the Witwatersrand, Johannesburg, South Africa; McGM = McGregor Museum, Kimberley, South Africa (Morris, 1984); MNHN = Muséum national d'Histoire naturelle, Paris, France; MPIEVA = Max Planck Institute for Evolutionary Anthropology, Leipzig, Germany; PBC = Pretoria Bone Collection, Pretoria, South Africa (L'Abbé et al., 2005); PCM = Powell-Cotton Museum, Birchington-on-Sea, UK; UCT = Department of Archaeology of the University of Cape Town, South Africa; ZSM = Zoologische Staatssammlung München, Germany.

[c] CBC = Cambridge Biotomography Centre (Nikon XT 225 ST Metris scanner) in the Department of Zoology at the University of Cambridge, Cambridge, UK; ESI = microfocus X-ray tomography facility (Nikon XT H225/320L industrial XCT system) at the Evolutionary Studies Institute of the University of the Witwatersrand, Johannesburg, South Africa; MNHN = AST-RX: X-ray tomography technical platform (v|tome|x L 240-180 equipment) at the Muséum national d'Histoire naturelle, Paris, France; MPIEVA = BIR ACTIS 225/300 industrial microfocus X-ray tomography scanner at the Department of Human Evolution in the Max Planck Institute for Evolutionary Anthropology, Leipzig, Germany; NECSA = MIXRAD microfocus X-ray tomography facility (Nikon XTH 225 ST Metris equipment) at the South African Nuclear Energy Corporation SOC Ltd, Pelindaba, South Africa.

SOM Table S2

Inventory, taxonomy, chronology, depository, and scanning information for the investigated fossil hominid and hominin specimens.

Specimen	Side	Taxon	Chronology/provenance	Collection[a]	Scan location[b]	Voxel size (µm)
IPS41724[c]	R	*Dryopithecus fontani*	Middle Miocene/Abocador de Can Mata, Vallès-Penèdes Basin, Spain	ICP	UBU	40
IPS18800.28[c]	L	*Hispanopithecus laietanus*	Late Miocene/Can Llobateres 2, Vallès-Penèdes Basin, Spain	ICP	UBU	40
IPS18800.29[c]	R	*Hispanopithecus laietanus*	Late Miocene/Can Llobateres 2, Vallès-Penèdes Basin, Spain	ICP	UBU	40
RUD 183[c]	R	*Rudapithecus hungaricus*	Late Miocene/Rudabánya, Hungary	MBFSZ	MPIEVA	30
RUD 234	L	*Rudapithecus hungaricus*	Late Miocene/Rudabánya, Hungary	MBFSZ	MPIEVA	30
MLD 46[c]	L	*Australopithecus africanus*	Plio-Pleistocene/Makapansgat, South Africa	ESI	MPIEVA	55
StS 14[c]	L	*Australopithecus africanus*	Plio-Pleistocene/Sterkfontein Member 4, South Africa	ESI	MPIEVA	41
StW 99	R	*Australopithecus africanus*	Plio-Pleistocene/Sterkfontein Member 4, South Africa	ESI	MPIEVA	91
StW 367	R	*Australopithecus africanus*	Plio-Pleistocene/Sterkfontein Member 4, South Africa	ESI	MPIEVA	91
StW 522[c]	R	*Australopithecus africanus*	Plio-Pleistocene/Sterkfontein Member 4, South Africa	ESI	MPIEVA	33
SK 82[c]	R	*Paranthropus robustus*	Early Pleistocene/Swartkrans Member 1, South Africa	Ditsong	MPIEVA	30
SK 97	R	*Paranthropus robustus*	Early Pleistocene/Swartkrans Member 1, South Africa	Distong	MPIEVA	30
KNM-ER 738	R	*Paranthropus boisei*?	Early Pleistocene/Koobi Fora Formation, Kenya	NMK	MPIEVA	38
KNM-ER 1465	L	*Paranthropus boisei*?	Early Pleistocene/Koobi Fora	NMK	MPIEVA	31

			Formation, Kenya			
KNM-ER 3728[c]	L	*Paranthropus boisei*?/ *Homo* sp.?	Early Pleistocene/Koobi Fora Formation, Kenya	NMK	MPIEVA	35

Abbreviations: R = right; L = left.

[a] Ditsong = Ditsong National Museum of Natural History, Pretoria, South Africa; ESI = Evolutionary Studies Institute of the University of the Witwatersrand, Johannesburg, South Africa; ICP = Institut Català de Paleontologia Miquel Crusafont (ICP) in Sabadell, Spain; MBFSZ = Mining and Geological Survey of Hungary, Budapest; NMK = National Museums of Kenya, Nairobi.

[b] MPIEVA = BIR ACTIS 225/300 industrial microfocus X-ray tomography scanner set at the Department of Human Evolution of the Max Planck Institute for Evolutionary Anthropology, Leipzig, Germany; UBU = industrial-CT YXLON Compact at the Human Evolution Lab. (LEB) at the Universidad de Burgos.

[c] The poor inner preservation of the region of interest in these specimens (SOM Fig. S1) excluded them from analyses

SOM Table S3

Results of pairwise Wilcoxon rank sum tests for estimates of calcar femorale length and height between the extant human (n = 9), *Pan* (n = 6), and *Gorilla* (n = 6) samples.[a]

Measurement[b]	Absolute values		Standardized values	
	Pan	*Gorilla*	*Pan*	*Gorilla*
PT MaxLength				
Extant humans	**0.0056**	0.3939	0.2721	**0.0003**
Pan	—	0.6991	—	**0.0043**
CF MaxLength				
Extant humans	**0.0016**	0.2721	0.1797	**0.0007**
Pan	—	0.4848	—	**0.0259**
CF MaxHeight				
Extant humans	**0.0004**	**0.0008**	**0.0007**	**0.0004**
Pan	—	**0.0260**	—	0.1797

CF = calcar femorale.

[a] Significant differences ($p < 0.05$) are in bold.

[b] PT MaxLength is measured from the periosteal contour; CF MaxLength is measured from the endosteal contour. See also Figure 2.

SOM Table S4

Means (or individual value), sample sizes (*n*), and ranges of absolute (in mm) and standardized estimates of the maximum width of the calcar femorale root measured in the extant human, *Pan*, and *Gorilla* samples and in one *Pongo* individual.

Taxon	Absolute values	Standardized values[a]
Extant humans	5.5	0.10
(*n* = 8)	3.7–9.1	0.05–0.14
Pan	5.8	0.14
(*n* = 5)	4.6–7.5	0.10–0.18
Gorilla	8.7	0.08
(*n* = 5)	4.8–10.1	0.04–0.15
Pongo (*n* = 1)	3.6	0.04

[a] Absolute values were standardized by body mass estimated for each individual from their femoral head diameter using the equations provided by Ruff et al. (2018, for humans) and Burgess et al. (2018, for apes).

SOM Table S5

Means (or individual value), sample sizes (*n*), and ranges of cortical bone thickness (CBT) measured at the anterior (CBTa) and posterior (CBTp) limits of the calcar femorale (CF) root on a transverse virtual section across the lesser trochanter at the level of the maximum width of the calcar femorale root in the extant human, *Pan*, and *Gorilla* samples and in one *Pongo* individual (see also SOM Fig S2).

Taxon	CBT (mm)
Extant humans	4.1
(*n* = 8)	3.5–6.1
Pan	3.4
(*n* = 5)	2.5–4.0
Gorilla	4.1
(*n* = 5)	3.0–5.8
Pongo (*n* = 1)	7.1

SOM Table S6

Results of partial Spearman's correlation test, controlling for body mass, between average cortical bone thickness and estimates of length, height, and calcar femorale (CF) root width.[a]

Measurement	Rho (*p*-value)[b]
PT MaxLength	0.49 (**0.04**)
CF MaxLength	0.29 (0.25)
CF MaxHeight	0.12 (0.63)
CF root width	-0.33 (0.17)

[a] PT MaxLength is measured from the periosteal contour; CF MaxLength is measured from the endosteal contour. See also Figure 2, SOM Figure S2, and SOM Table S4.

[b] Significant differences ($p < 0.05$) are in bold.

SOM Table S7

Results of the Spearman's rank correlation tests between estimated body mass and calcar femorale (CF) length and height in the extant human (n = 9), *Pan* (n = 6), and *Gorilla* (n = 6) samples.

Measurement[a]	Rho (p-value)[b]
PT MaxLength	0.35 (0.11)
Extant humans	0.33 (0.39)
Pan	-0.37 (0.50)
Gorilla	0.67 (0.18)
CF MaxLength	0.35 (0.12)
Extant humans	0.07 (0.88)
Pan	-0.14 (0.80)
Gorilla	-0.03 (1.00)
CF MaxHeight	0.35 (0.12)
Extant humans	0.53 (0.15)
Pan	-0.26 (0.66)
Gorilla	-0.43 (0.42)

[a] PT MaxLength is measured from the periosteal contour; CF MaxLength is measured from the endosteal contour. See also Figure 2.

[b] None of the correlations are significant ($p > 0.05$)

SOM References

Burgess, M.L., McFarlin, S.C., Mudakikwa, A., Cranfield, M.R., Ruff, C.B., 2018. Body mass estimation in hominoids: Age and locomotor effects. J. Hum. Evol. 115, 36–46.

L'Abbé, E.N., Loots, M., Meiring, J.H., 2005. The Pretoria Bone Collection: A modern South African skeletal sample. Homo 56, 197–205.

Morris, A.G., 1984. Osteological analysis of the proto-historic populations of the Northern Cape and Western Orange Free State, South Africa. Ph.D. Dissertation, University of the Witwatersrand.

Ruff, C.B., Burgess, M.L., Squyres, N., Junno, J.A., Trinkaus, E., 2018. Lower limb articular scaling and body mass estimation in Pliocene and Pleistocene hominins. J. Hum. Evol. 115, 85–111.